# FLUIDIC DIELECTROPHORESIS: POLARIZATION AND MANIPULATION AT LIQUID/LIQUID INTERFACES

By

Mitchell Desmond

A thesis submitted to Johns Hopkins University in conformity with the requirements for the degree of Master of Science Engineering

Baltimore, Maryland

August, 2014

# Abstract

This work presents a new type of alternating current (AC) interfacial polarization and frequency dependent fluid displacement phenomenon at a liquid/liquid electrical interface and how it can be used for microfluidic control. We used two fluid streams, one with a greater electrical conductivity and the other a greater dielectric constant, and flow focused them side-by-side in a microfluidic channel. By using gold electrodes aligned with the microchannel, we applied an AC electric field perpendicular to the interface, and fluid is observed to displace across the liquid/liquid interface. The direction and magnitude of this displacement is frequency dependent. At low AC frequency, below the interfacial inverse charge relaxation time, the high conductive fluid displaces into the high dielectric stream. At high frequency the direction of liquid displacement reverses, and the high dielectric stream injects into the high conductivity stream. The interfacial crossover frequency where the liquid displacement direction reverses is dependent on differences in electrical properties between the two fluid streams, and is well explained by Maxwell-Wagner polarization mechanics.

We demonstrate how the interfacial crossover frequency of a liquid/liquid interface can be measured using impedance spectroscopy. We added an interdigitated gold electrode design downstream from electrodes used for fluid displacement. The impedance of the liquid/liquid interface was characterized over a frequency range of 1kHz to 7 MHz with no fluid displacement. When we apply low frequency to the upstream electrodes to displace the high conductive stream, the impedance decreases, and at high frequency when the low conductive stream displaces, the impedance increased. We determined that the optimum frequency to record impedance on the sensor electrodes

to be 400 kHz. By measuring the impedance of the sensor electrodes at this fixed frequency, and sweeping the function generator to displace the interface, the crossover frequency can be quickly determined from the resulting LabView graph.

We also demonstrate how fluidic dielectrophoresis can be used to make an active mixing device in a in a microfluidic system. When two high conductive streams are displaced simultaneously into a center low conductive stream we can create micro-vortices and cause the system to mix on a $\mu$s time scale. The two advantages of this device are the speed of mixing, which can be turned on or off very quickly, and the voltage dependence of the mixing, that can be used for tunable injection. This technique keeps the mixing volume constant and can be achieved in a very short distance in the microfluidic channel.

Finally, we demonstrate how the mixing device mentioned above can be applied upstream to a chemotaxis device to create instant gradient control. Based on the voltage dependent mixing of a high conductive stream with a lower conductive stream in an AC field we were able to produce tunable spatial chemical gradients with arbitrary geometry and solute concentration steepness in a microfluidic device for studying directed cell migration. When the electric field is turned on, the high conductive cell buffer mixes with the low conductive buffer and is sent down stream. When the field is off the high conductive cell buffer exits the chip before the chemotaxis chamber. By adding cyclic adenosine monophosphate (cAMP) to the high conductive buffer we can control the strength and direction of the cAMP chemical gradient in the chemotaxis chamber. To change the direction of the chemical gradient, the applied voltage is switched from the electrodes on the first inlet to the electrodes on the second inlet.

## Table of Contents

# List of Figures

# Preface

This thesis was made possible with the help and support of a number of individuals. Most importantly, my mentor and primary investigator, Dr. Zachary Gagnon, was extremely helpful. Nicholas Mavrogiannis was in the lab with me from the very beginning and helped me with many experiments. Huy Vo taught me everything I know about fabrication. Thank you to Michael Bevan for reading my thesis and giving me advice on running experiments.

# Introduction

The action of the electric field on the induced charge gives rise to electrical forces and forms the basis for many types of electrokinetic phenomena including particle dielectrophoresis (1) and liquid electro-osmosis (2). The charging mechanism, known as Maxwell-Wagner (MW) polarization (1), has been exploited to pump liquid (3,4) (electro-osmosis), and manipulate bubbles (5), particles (6), biomolecules (7),(8) and cells (9) (dielectrophoresis). Research and application in this area, however, has been primarily limited to interfaces formed between two or more immiscible surface-liquid, particle-liquid, or gas-liquid phases. While there has been work done with direct current (DC) electric fields at liquid/liquid interfaces (10,11), the influence of an alternating current (AC) electric fields applied perpendicular to a liquid/liquid electrical interface remains unexplored. Our first goal is to characterize the effects of AC polarization at an electrical interface formed between two miscible aqueous liquids. We demonstrate that an aqueous electrical interface exposed to a perpendicular AC electric field undergoes frequency dependent polarization and liquid displacement well described by MW polarization mechanics.

An emerging new technology for point of care testing is microfluidic devices that perform various chip-based chemical and biological analyses. The benefits of using lab on a chip (LOC) technology is higher throughput, shorter analysis times, reduced sample volumes, the possibility for in situ operation, and reduced operation and manufacturing costs. Impedance spectroscopy in microfluidic devices has been used for biological assays by creating a chemical reaction at the electrode surface (12). The problem with

this design is that fabrication is difficult and the surface reaction is used up almost immediately. We demonstrate a novel impedance detection design that can be used in a microfluidic device to continuously monitor the changes at a liquid/liquid interface. Our second goal is to characterize the effects of fluidic dielectrophoresis on an impedance sensor. This sensor can then be used to determine the interfacial position and crossover frequency of the system.

A primary goal of LOC technology is to miniaturize bio-analytical systems used in typical laboratory settings onto a small portable device. The rate-limiting step for many of these miniaturized processes is the mixing because of the low rate of diffusive transport at the micro scale. Immunoassays, DNA hybridization, and general cell-molecule interaction all require rapid mixing for analysis. We demonstrate how two high conductive streams can be deflected into a center low conductive stream, using a low frequency AC field, to create rapid mixing on the micro scale. Our third goal is to characterize the effects of frequency and voltage on the mixing of three laminar streams.

Chemotaxis is the phenomenon where cell movement is directed in response to an extracellular chemical gradient and plays a crucial role in the recruitment of inflammatory cells to sites of infection, and organ development during embryogenesis. In cancer, chemotaxis pathways can be reprogrammed in favor of tumor cell dissemination, known as cancer metastasis (13). Researchers have studied chemotaxis behavior with Zigmond chambers and needle assays that rely on chemical diffusion and static concentration gradients. Recently, lab on a chip (LOC) devices for chemotaxis studies have been developed in order to collect more quantitative data and to take advantage of faster experiments, higher sensitivity and improved gradient control (14). While current

chemotaxis assays are effective in quantifying biased cell migration, current methods produce static chemical gradients that are fixed in terms of concentration steepness; on-chip concentration levels can only be modified by manually modifying off-chip samples (14). Currently, no device exists that provides fast, precise, and tunable chemical gradient concentration control for the study of chemotaxis. We demonstrate how the electrode design used for fluidic dielectrophoresis can be placed upstream in a chemotaxis device to create tunable chemical gradients in the cell chamber. Our fourth goal is to characterize how the voltage dependent injection of more conductive cell buffer into a chemotaxis device changes the chemical gradient that is felt by the migrating cells.

# Background

## Maxwell-Wagner Polarization

When an electric field is applied across the interface between two materials with disparaging electrical conductivity ($\sigma$) and dielectric constant ($\varepsilon$), such as an insulating particle suspended in conductive electrolyte, surface charge will accumulate and the interface will polarize. When an alternating current (AC) electric field is applied across the interface the magnitude and sign of the induced charge is frequency ($\omega$) dependent. At low AC frequency, below the inverse charge relaxation time ($\varepsilon/\sigma$), material with greater conductivity conducts ionic charge to the interface at a rate faster than it is removed by the adjacent lower conductive phase (1). As such, charge accumulates at the interface, and low frequency interfacial polarization is driven by material differences in electrical conductivity as shown in figure 1 below.

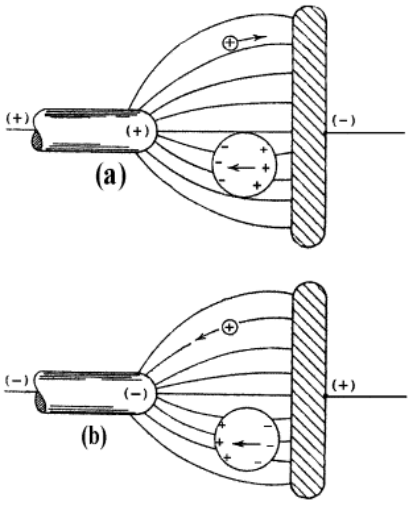


Figure 1: Dielectrophoresis of a particle in a non-uniform AC field. Diagram (a) shows the polarized particle in traveling towards the positive lead. When the field is switched in diagram (b) the particle travels in the same direction because the frequency was slow enough to allow the charges in the particle to re-orient.

At high frequency, above the charge relaxation timescale, the electric field oscillates faster than charges can re-orient to the interface. As conductive charging does not have enough time to occur over every field half-cycle, high frequency polarization is driven by differences in material dielectric constant; charge accumulates due to interfacial differences in dielectric polarization. If neither interfacial phase has both a greater electrical conductivity and dielectric constant, the high conductivity phase dominates interfacial charging at low frequency and the adjacent high dielectric phase drives charging at high frequency. Hence, the net sign of the induced interfacial charge reverses at a frequency high enough to relax away conductive charging to the extent that it is trumped by opposing dielectric polarization. This frequency is on the order of the inverse charge relaxation timescale, and is defined as the crossover frequency (COF).

This concept can be applied to a liquid/liquid interface by flow focusing two fluids in microchannel. In the figure 2 presented below, the green stream has a high conductivity and low permittivity, while the red stream has a low conductivity and high permittivity.

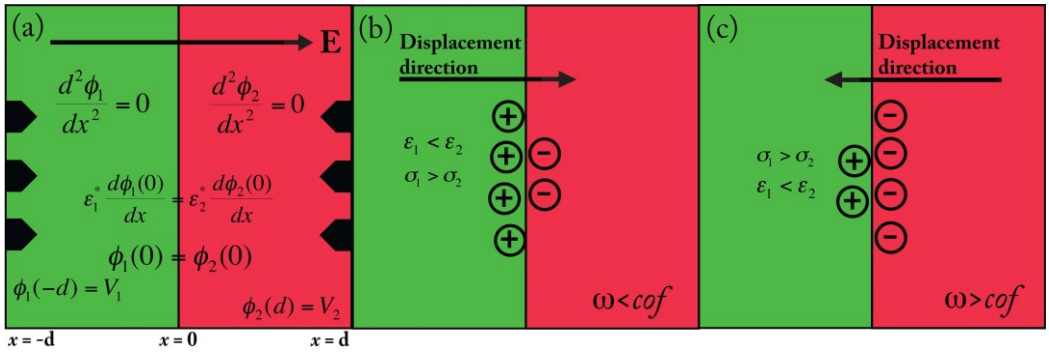


Figure 2: Polarization of the liquid/liquid interface. (a) The electric field is off and the interface is stable. The green stream represents PBS and has a high conductivity and low permittivity. The red stream represents AHA and has a low conductivity and high permittivity.

Assuming each fluid is electro-neutral, the electric potential in each phase very near the channel surface is well described by the one-dimensional Laplace equation in $x$,

$$\frac{d^2\phi_i}{dx^2} = 0 \tag{1}$$

where $\phi_i$ is the applied potential in the i$^{th}$ liquid stream, 1 (green) and 2 (red), and $x$ points in the direction normal to the electric interface. We apply the usual MW boundary conditions at the electrical interface between the two liquid streams. First, as illustrated in figure 2, we require the electric potential across the electrical interface ($x$=0) be continuous, $\phi_1(0) = \phi_2(0)$. Second, accounting for both ohmic current (conductive polarization) and displacement current (dielectric polarization) across the interface, we require continuity in displacement current:

$$\varepsilon_1^* \frac{d\phi_1}{dx} - \varepsilon_2^* \frac{d\phi_2}{dx} = 0 \tag{2}$$

$$\varepsilon_i^* = \varepsilon_i - \frac{i\sigma_i}{\omega} \tag{3}$$

where $\varepsilon_i^*$ is the complex permittivity in each liquid phase. Hence, the fluid interface is subject to a net charge accumulation due to a discontinuous jump in conductivity and dielectric constant in order to satisfy the conservation of both ionic and dielectric charge (1). Using the above conditions, combined with boundary conditions for the applied potential,

$$\phi_1(-d) = V_1 \tag{4}$$

$$\phi_2(d) = V_2 \tag{5}$$

where $V_1$ and $V_2$ are the applied potential at each electrode ($x = \pm d$), the Laplace equation in both liquid domains is solved. The interfacial *cof* occurs at an AC frequency where conductive charging completely balances dielectric polarization, and the net charge across the interface is zero. This condition occurs when the normal electric field ($E_n = {\phi_i}/{dx}$) is continuous across the liquid/liquid interface,

$$\frac{d\phi_1}{dx} - \frac{d\phi_2}{dx} = f = 0 \tag{6}$$

Based on the two-domain solution to the 1D Laplace equation, this liquid interfacial *cof* occurs when

$$f(\omega) = \frac{\varepsilon_1^* - \varepsilon_2^*}{\varepsilon_1^* + \varepsilon_2^*} = 0 \tag{7}$$

It is important to note that $f(\omega)$ is a complex function, and has both real (in-phase with the applied field) and imaginary (out of phase) parts. In this work, we apply the electric field as a single sinusoid, so there is no phase gradient, and charging is driven by the in-

phase component (real part) of the electric field (1). Hence, the predicted crossover frequency ($\omega_{co}$) where induced interfacial charge vanishes is determined by the real part of $f(\omega)$, or in functional form:

$$\omega_{co} = \frac{1}{2\pi}\left[\frac{(\sigma_1-\sigma_2)(\sigma_1+\sigma_2)}{(\varepsilon_2-\varepsilon_1)(\varepsilon_1+\varepsilon_2)}\right]^{1/2} \tag{8}$$

Based on equation 8 we can calculate the theoretical COF for changes in conductivity for the two streams. The predicted crossover is plotted in figure 3 below as a function of the electrical conductivity difference between stream 1 and 2, $[\sigma_1 - \sigma_2]$, holding all other electrical properties constant.

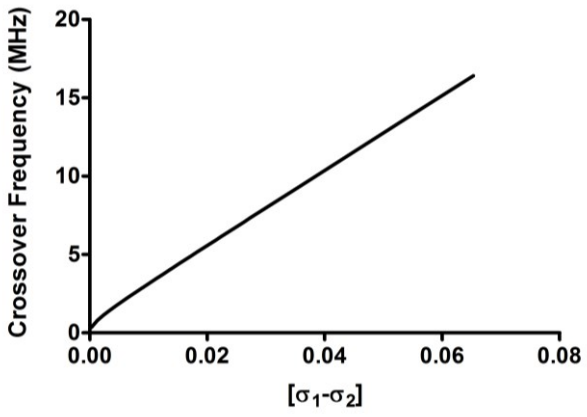


Figure 3: Theoretical COF vs. liquid/liquid interface conductivity difference. This graph shows how the COF increase as the difference in conductivity of two streams increases while all other electrochemical properties are held constant.

The predicted COF for changes in permittivity between the two streams can also be determined using equation 8. The predicted crossover is plotted in figure 4 below as a function of the electrical permittivity difference between stream 1 and 2, $[\varepsilon_2 - \varepsilon_1]$, holding all other electrical properties constant.

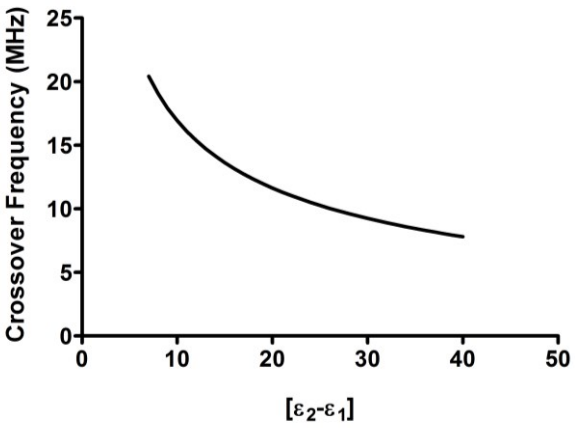


Figure 4: Theoretical COF vs. liquid/liquid interface permittivity difference. This graph shows how the COF decreases as the difference in permittivity between the two graphs increases.

## Impedance Analysis

Impedance (Z) is defined as the total opposition a circuit offers to the flow of an alternating current (AC) at a given frequency. Impedance is a complex number and is represented as

$$Z = R + jX \tag{9}$$

where R is the real part called resistance, and X is the imaginary part called reactance. Resistance and reactance are graphed as an ordered pair of numbers on a vector plane in figure 5 below where $|Z|$ is the vector with phase angle $\theta$ (15).

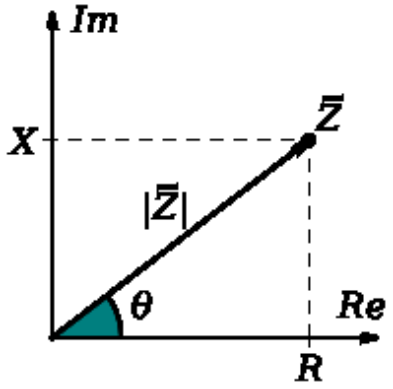


Figure 5: Graphical Representation of Impedance (Z). Impedance is a complex number with a real part represented on the x-axis as resistance (R) and an imaginary part on the y-axis represented as reactance (X).

Based on figure 5, the mathematical relationship between the impedance values can be deduced as:

$$Z = \sqrt{R^2 + X^2} \tag{10}$$

$$R = |Z| \cos\theta \tag{11}$$

$$X = |Z| \sin\theta \tag{12}$$

Reactance is the opposition of a circuit element to a change of electrical current or voltage, due to that elements inductance or capacitance. The equations for the capacitive reactance ($X_c$) and the inductive reactance ($X_L$) are defined as

$$X_C = 1/(2\pi f C) \tag{13}$$

$$X_L = 2\pi f L \tag{14}$$

where $f$ is the frequency that is applied, C is the capacitance, and L is the inductance. Capacitive reactance is the opposition to the change of voltage across an element. A DC voltage applied across a capacitor causes positive charge to accumulate on one side and negative charge to accumulate on the other side; the electric field due to the accumulated

charge is the source of the opposition to the current. When the potential associated with the charge exactly balances the applied voltage, the current goes to zero. When an AC supply is used, a capacitor will only accumulate a limited amount of charge before the potential difference changes polarity and the charge dissipates. The higher the frequency, the less charge will accumulate and the smaller the opposition to the current. Inductave reactance is an opposition to the change of current through an element and is proportional to the frequency through an element. All capacitors in an AC circuit have a finite amount of inductance. In an ideal resistor there is no reactance and the impedance is given as just R. In an ideal capacitor or inductor there is no resistance, and impedance is given as just X. However, in a real system there are no pure R, C, and L components. Parasitics means that all real world circuit components have both resistance and reactance. Resistors have unwanted inductance, capacitors have unwanted resistance, inductors have unwanted capacitance, etc. The amount of parasitics that exists in an elements is dependent on the design and manufacturing (15).

An equivalent circuit refers to a theoretical circuit that retains all of the electrical characteristics of a given circuit. An equivalent circuit simplifies calculations, and can represents a more complex circuit in order to aid analysis. An equivalent circuit can also be used to represent the electrical characteristics of a system that is not a defined circuit, like a biological system. The membrane of a cell can be modeled with an equivalent circuit where a capacitor and resistor in series represent the lipid bilayer. If the impedance characteristics of any system are known over a frequency range, an equivalent circuit model can be developed for that system to better understand how the system works in terms of R, C, and L. When making an equivalent circuit model it is important

to consider parasitics for all components. Often times a simple component has to be represented as a complex circuit, as shown in figure 6 below (16).

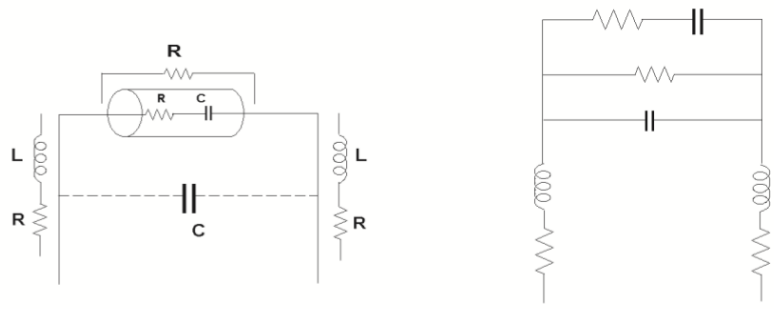


Figure 6: Equivalent circuit model for a capacitor. The equivalent circuit for a system can only be confirmed after the impedance is measured over a specific frequency range. There are an infinite number of possible equivalent circuit models for a single capacitor, but only one design will fit the measured impedance with the least amount of error.

## Microfluidic Mixing

There are two classes for integrated on chip mixing, passive and active. Passive devices rely on the fluid transport mechanism to create flows for mixing. The liquids to be mixed are pumped through a channel with baffles or obstacles that create twisting pathways (17). This method creates mixing by stretching the interface between the liquids and decreasing the distance over which diffusion must take place to provide a uniform mixture. This method creates a very disperse sample. The sample is diluted because the volume continuously increases as it spreads out longitudinally during the passive mixing processes. The Christmas tree gradient generator is a very common passive mixing device that has a slow response time for changes in gradient concentration. Furthermore, any gradient concentration change has to be done off chip in the sample solution.

Active mixing devices generally have shorter mixing length and mixing times because they use an external driving force. Electrokinetic force is a promising way to create chaotic advection to enhance mixing. When using DC voltage, a charge layer builds up and shields the liquid interface. DC electroosmotic flow can require hundreds to thousands of volts for actuation. In contrast, an AC electric field with low frequency can charges the interface faster then the charge relaxation time and there is no charge buildup on the walls. Current microfluidic mixing designs focus on lower voltage and higher frequency to reduce electrolytic reactions on the surface of the electrodes (17).

# Materials and Methods

## Fabrication

The microfluidic device utilized in this study were fabricated using standard soft lithography and microfabrication techniques (18,19). An outline of this process is presented below in figure 7.

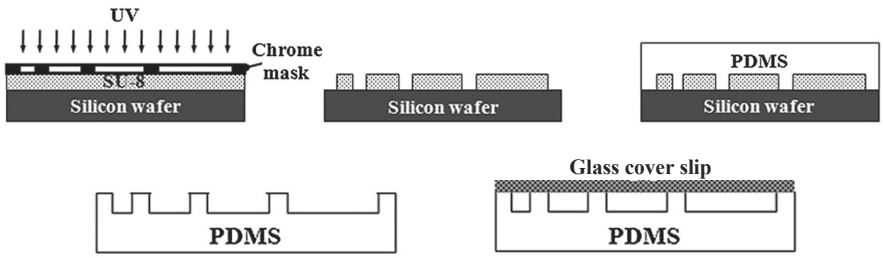


Figure 7: Summary of soft lithography process. UV light is used to cure the photoresist through a mask and PDMS is poured over the mold that is made from developed photoresist. The PDMS is taken off the wafer and bonded to glass.

After spinning photorsesist onto the wafer we used a mask aligner to expose the Su-8 to UV light through a printed mask design. UV light makes the SU-8 photoresist insoluble in developer. The design from the mask is left on the silicone wafer with the height that the photoresist was spun on. A 1:10 mixture of PDMS elastomer (Momentive, RTV 615A) and curing agent is poured atop a lithographically fabricated SU-8 polymer mold, cured and gently peeled off. Fluid ports are punched into the PDMS using a 0.75mm biopsy punch (Ted Pella, Inc.). Microchannel electrodes are fabricated using wet chemical etching. Glass cover slips (50x30mm - #1, Fisher Scientific) are coated with 2 nm of titanium and 50 nm of gold using electron beam evaporation. The cover slips are then patterned with photoresist (Shipley 1813) and the exposed metal film is etched away with titanium and gold chemical etchant creating an array of patterned metal electrodes.

The microchannel and coverslip are exposed to oxygen plasma (Jelight, Model 42A) and immediately aligned and sealed under an inverted microscope (19).

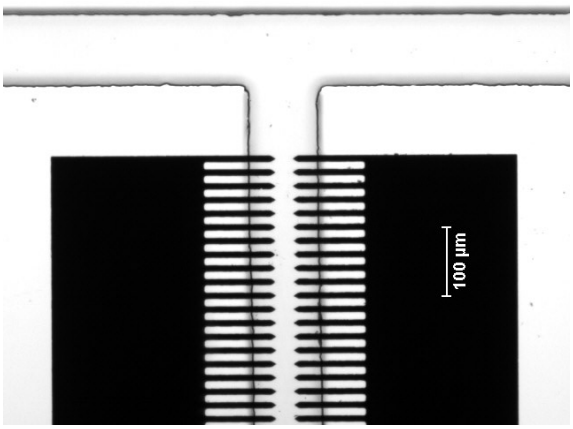


Figure 8: Bright field image of aligned electrode and microchannel device. The electrodes (shown in black) are on the surface of the glass cover slip and the PDMS T channel is aligned on top using a stereoscopic microscope.

As shown in Figure 8 above, the device consists of a main flow channel 100 μm wide and 65 μm high. The embedded electrodes are axially separated by 20 μm and symmetrically bridge the channel width. Here, electrodes with sharp points are utilized in order to maximize the electric field strength across the liquid interface, as the sharp point serves to focus the electric field to the tip of the electrode.

## Fluidic Dielectrophoresis

Due to the laminar flow profile and slow diffusion timescale associated with low Reynolds number flow, two liquids of differing electrical properties can flow side-by-side in a microchannel and create a sharp electrical discontinuity at their contacting interface, as seen in the 3D confocal image of the main flow channel blow in figure 9.

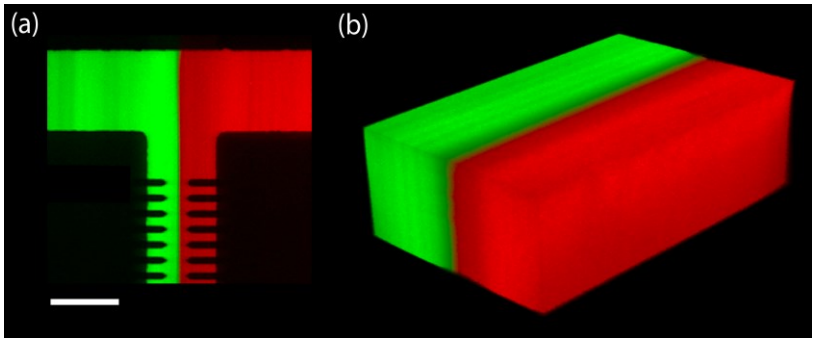


Figure 9: confocal image of T channel and confocal Z-stack of fluid flow. With the Nikon swept field confocal microscope we can image up to 4 florescence at the same time. Using a triggered piezo-z stage we can create z-stack images shown in (b).

The electrical interface is readily observed and imaged by labeling each fluid stream with soluble red and green fluorescent dye. The resulting fluorescent interfacial cross-section [Fig. 9 (b)] is captured using a confocal microscope (Nikon/Prairie Technologies) equipped with an Andor iXon 897 camera, two 50 mW solid-state lasers for excitation at 488 nm and 561 nm. The left-most (green) high conductivity stream consists of diluted 10X phosphate buffered saline (PBS) labeled with 10 ng/mL of Alexa Fluor 488 (Invitrogen). The right-most (red) high dielectric stream consists of 2M 6-aminohexanoic acid (Sigma-Aldrich) (AHA) labeled with 10 ng/mL of Alexa Fluor 594 (Invitrogen). AHA is a water-soluble zwitterion used for increasing the dielectric constant of aqueous solution (20). Prior to fluorescent labeling, the AHA solution is vigorously shaken for 5 minutes in 5 g/mL Dowex MR-3 (Sigma) ion exchange resin to remove trace salts and reduce solution conductivity (20). The electrical conductivity and dielectric constant of each liquid phase is readily measured with a handheld conductivity meter and LCR impedance analyzer, respectively. For all experiments the samples are pressure injected into the microfluidic device at a steady flow rate of 100 μL/min. A

function generator (Rigol, DG2041A) is wired to the embedded electrodes and used to deliver an AC electric field across the liquid/liquid interface. To achieve higher voltage, an amplifier unit was attached to the function generator increasing the AC field to 50V.

## Impedance Analysis

To measure the impedance of the liquid/liquid interface we used an interdigitated gold electrode design. We incorporated this second electrode desing into a microfluidic T channel below the electrodes that we used for fDEP. The electrode designs, with the flow T channel, are shown below in figure 10.

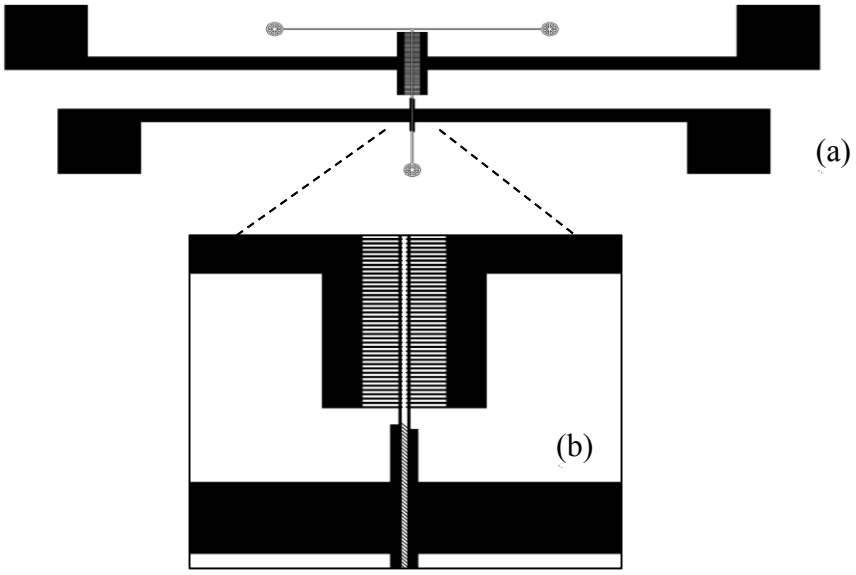


Figure 10: Impedance sensor design and completed LOC device. The gold electrodes on the sensor are fabricated the same way the electrodes were fabricated for studying fDEP.

We fabricated the sensor electrodes the same way the previous gold electrodes were fabricated for fDEP. The same cover slip size and gold deposition process were used. The fDEP electrodes and sensor electrodes are etched on the cover slip at the same

time. Our chip has two separate sets of gold pads to wire the function generator and the impedance analyzer to the top fDEP electrodes and bottom sensor electrodes respectively. To ensure a strong electrical connection we used indium solder to connect wires to the device.

We used a HP4192A impedance analyzer to characterize our system. This impedance analyzer is capable of sweeping through a given frequency range and recording the measured impedance at each frequency, or measuring impedance continually at a fixed frequency. To measure impedance we needed to record two values, either Z and $\theta$, or R and X. To record the measurements from the impedance analyzer we used LabView programs downloaded from National Instruments website. We edited the LabView programs so that they could send the recorded data to an excel file, shown below in figure 11.

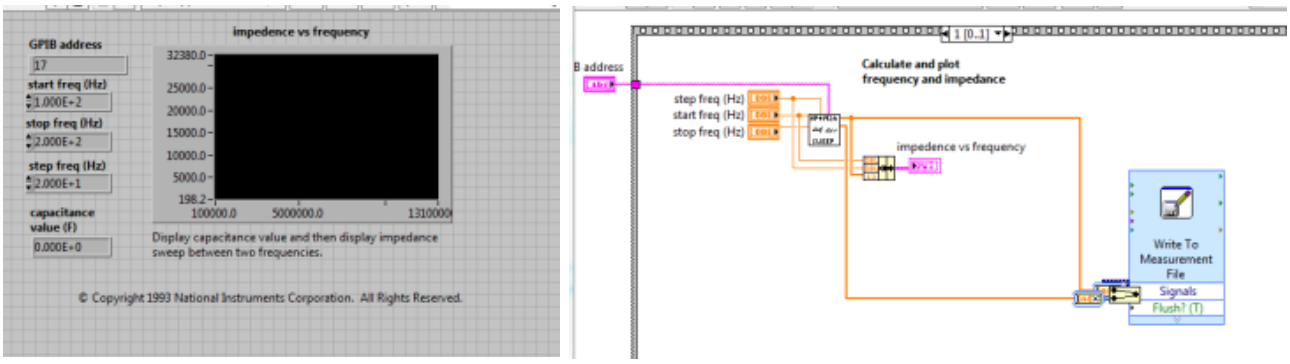


Figure 11: LabView impedance sweep program. We used this program to sweep over a frequency range with a given frequency step size. For each frequency a impedance (Z) and phase angle ($\theta$) measurement were take.

We used a second program to record impedance continuously at a fixed frequency. The impedance is graphed in a waveform chart against time and the data is exported to an Excel file after the program is stopped. The user interface and program are shown below in figure 12.

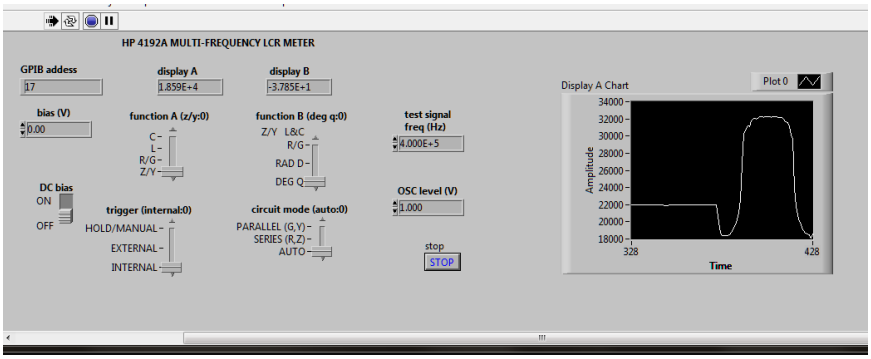


Figure 12: Continuous impedance measurement LabView program. LabView measures impedance at one frequency and the value of $|Z|$ is recorded against time as the measurements are recorded in a waveform chart.

To connect the sensor electrode pads to the impedance analyzer we used a two terminal configuration of wires purchased from National Instruments. The wire was exactly one meter long and we set the built in test fixture on the impedance analyzer to match the specifications of the test wire.

## Active mixer

To create an active mixing device, we used the same electrode design that was used to study fDEP and added a third inlet stream to the T channel design. The finished active mixing device and a confocal picture of the inlet are presented below in figure 13.

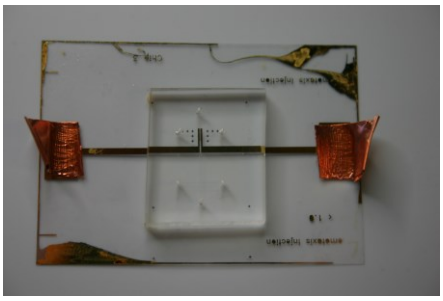

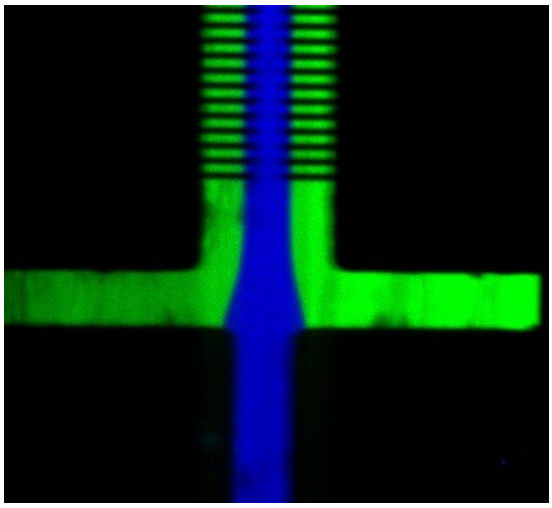

Figure 13: Active microfluidic mixing design. Three streams are flow focused down a channel that has been aligned with electrodes. The center stream (purple) is low conductive AHA solution and the two sides streams (green) are high conductive PBS solution. Right picture taken with confocal microscope and 10x objective.

We attached the electrode pads on the cover slip are attached to a function generator and a voltage amplifier with copper tape. The amplifier allows us to apply up to 50 volts AC at a fixed frequency between 100 kHz and 15 MHz.

## Tunable Chemotaxis device

To design a novel chemotaxis device, we took the fDEP fluid displacement design and integrated it into the upstream components of a microfluidic gradient generator. The gradient generated design we modified, called the ladder chamber, has two fixed inlets that create a static gradient in the horizontal microgrooves, as shown below in figure 14. With this device, one inlet stream has cAMP and the cells are loaded on the opposite side, and the gradient that forms forces the cells to migrate through the horizontal microgrooves (21).

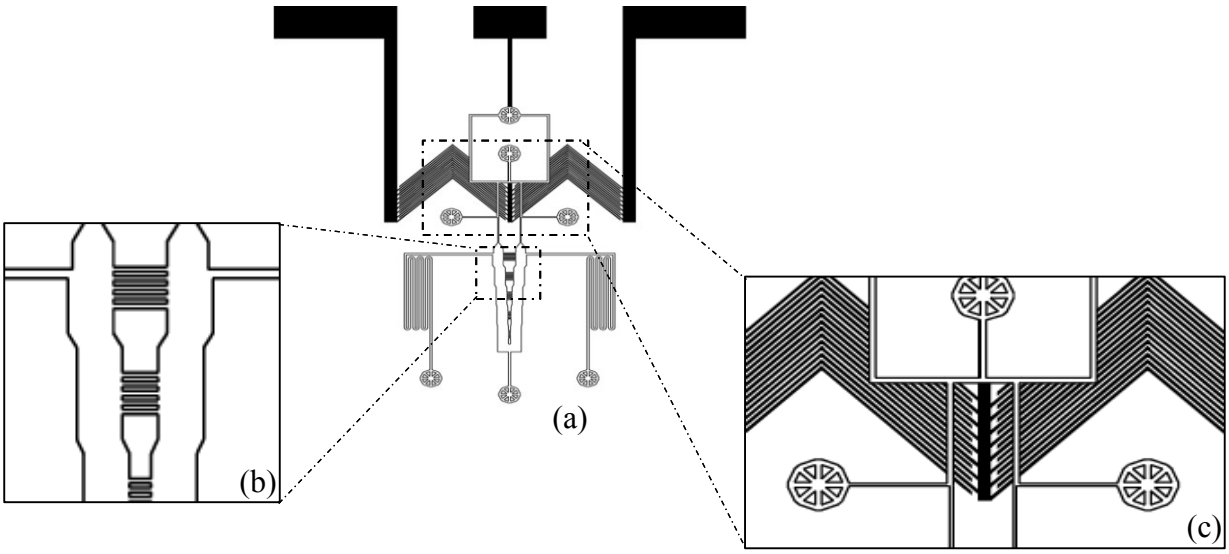


Figure 14: Electrode design for gradient generating device. (a) shows the overall device with interdigitated 45 degree electrodes in black and flow channel design outlined in black. (b) is a close up of the chemotaxis cross channels in the chip where the gradient forms. (c) is the inlet to the gradient chambers where the deflection occurs to control what fluid is sent downstream.

The modifications that we made are shown on the left in figure 14. We added two additional inlets and an fDEP electrode design to both sides. Originally we used the same electrode design that was mentioned earlier in the fDEP experiments, but we were not able to align the channels on both sides of the device with the two electrodes. We decided to use interdigitaded electrode design that allowed for more flexibility when aligning the channels. The green stream on either side is high conductive DB buffer with cAMP and the red solution is the diluted, low conductivity, DB solution. We lowered the conductivity of the red DB buffer by diluting it 1:1 with DI water. When the electric field is active, fluid is displaced into the other half of the channel and is passed downstream. If the electric field is removed, displacement will cease, and the fluid will exit the device without going downstream. When the first electrode module is switched on, a gradient forms in the horizontal microgrooves and is quickly removed when the

electric field is turned off. The gradient direction is switched by activating the electrode module on the opposite side. The concentration gradient presence and slope can both be calculated from an analysis of the florescence intensity in the chip using confocal microscopy.

# Results

## Characterizing FDEP

An electric field is applied across the liquid interface and fluid from one stream is observed to displace into the adjacent stream, seen in the cross-sectional confocal image captured at $\omega = 4$ MHz in figure 15 below.

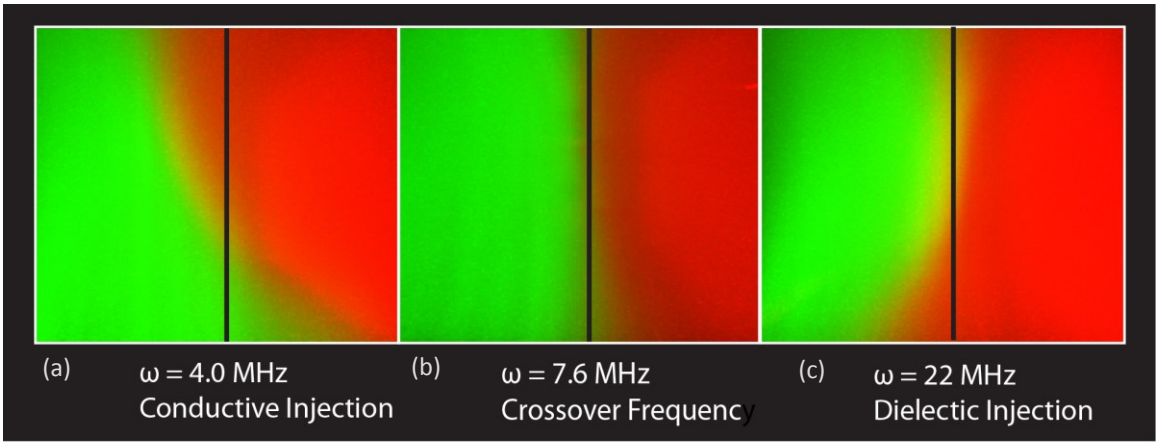


Figure 15: Cross-sectional channel images taken with confocal microscope. (a) At low frequency the more conductive stream displaces because of higher conductivity. (b) At the crossover frequency the interface has equal force on both sides and does not deflect. (c) At high frequency the high permittivity stream deflects.

A solid black line indicates the original interfacial position – the high conductivity stream (green) displaces across the interface into the neighboring high dielectric stream (red) at an AC frequency of 4 MHz. The frequency is slowly increased and the high conductive fluid continues to displace across the interface into the adjacent stream. At a frequency of 7.6 MHz, however, liquid displacement rapidly ceases [Fig. 15(c)], and the interface is visually identical to that as seen in figure 9 when no AC voltage is applied. The frequency is increased above 7.6 MHz and the displacement direction reverses; the

high permittivity stream ($\sigma$ = 19 μS/cm, $\varepsilon$ = 110) displaces into the adjacent high conductive stream [Fig. 15(d)]. Hence, a liquid interfacial *cof* is observed at 7.6 MHz. Below the *cof* the high conductive stream displaces into the high dielectric stream. Above this, the high permittivity stream displaces into the high conductive stream. Hence, the interface appears to "tilt" left or right, depending upon the AC frequency applied.

Cross-sectional views of the polarized interface taken by confocal microscopy illustrate how the observed field-induced liquid displacement satisfies conservation of mass.

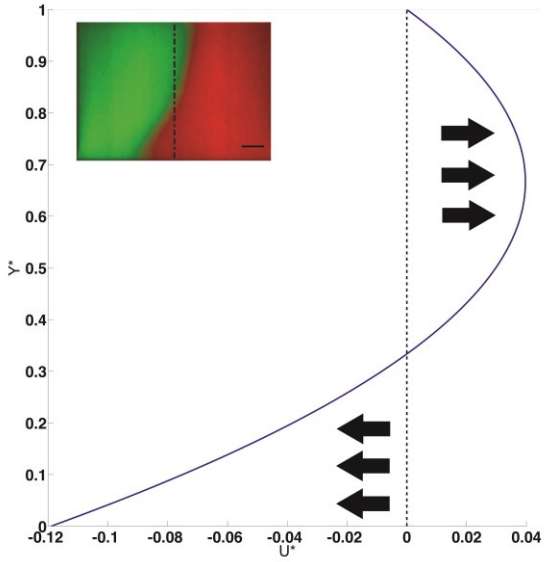


Figure 16: Cross section velocity profile illustrating the conservation of mass. When the fluid deflects at the bottom of the channel there is a resulting pressure force in the opposite direction. The graph shows the theoretical dimensionless velocity profile in the channel. There is a no slip condition at the top of the channel. The actual displacement profile is shown in the top left corner.

As the field-inducing electrodes exist solely on the bottom channel wall, symmetry is broken, and field-induced fluid displacement is largely driven by the interfacial Maxwell stress at the bottom channel surface where the electric field is largest. At high AC frequency (22 MHz), above the liquid *cof*, the low conductivity stream (red) displaces

across the channel into the high conductive stream (green). To accommodate for this volume exchange, the high conductive fluid (green) near the top channel wall displaces in the opposite direction. Here, a dotted black line indicates the original interfacial position when no field is applied.

It is important to note that when a series of control experiments are conducted, where each stream had identical electrical properties, no fluid motion is observed over the entire range of applied frequency or voltage (200 kHz – 25 MHz, 1 – 10 $V_{pp}$). Second, no liquid *cof* is observed when one single stream has both a larger conductivity and dielectric constant; the high conductive/dielectric stream displaces in a single direction for all frequencies applied. Fluid systems having only differences in one electrical property – either conductivity or permittivity – produced only fluid displacement in a single direction; no *cof* was observed. Finally, liquid displacement is extremely sensitive to differences liquid conductivity and dielectric constant between adjacent streams. A 0.05% difference in either parameter between each stream is all that is required to optically observe fluid motion with the confocal microscopy system used in this work.

Interfacial *cof* measurements were repeated over a large range of electrical conductivities of the high conductivity fluid stream (0.0029 – 0.61 mS/cm), while keeping all other electrical properties constant. An increase in *cof* is observed as the conductivity of the high conductivity phase is increased, shown by the data set plotted in figure 17 below.

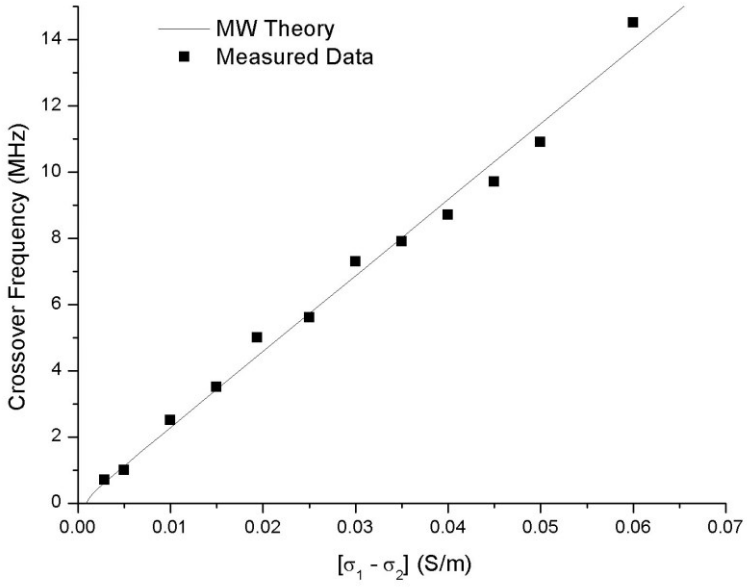


Figure 17: COF measurements plotted against theoretical COF data. We changed the conductivity of the PBS stream by diluting it with water and then measured the crossover frequency using confocal fluorescence measurements.

At low frequency, below the inverse charge relaxation time, the high conductive stream conducts ionic charge to the interface at a rate faster than can be removed by the adjacent low conductive liquid. As such, the high conductive fluid dominates the polarization of the interface. At high frequency, when ionic charging does not have enough time to occur, the high dielectric liquid governs the interfacial charging. Therefore, the net sign of the induced interfacial charge between the two liquids reverses depending upon the AC frequency applied, since neither liquid has both greater conductivity and dielectric constant. As charge reversal can occur, there exists an intermediate frequency where conductive charging is equally balanced by dielectric charging, and the interface has a zero net charge. The observed increase in *cof* with increasing differences in electrical conductivity is consistent with this argument.

Physically, as the difference in electrical conductivity between each fluid stream increases, the total amount of induced interfacial ionic charge increases, and a larger field frequency is required to relax the charge away. Hence, a larger crossover frequency is observed as the relative difference in electrical conductivity, $[\sigma_1 - \sigma_2]$, is increased. For three conductivity differences we measured the displacement across the channel for the frequency range 1MHz to 20 MHz at a fixed voltage. The resulting displacement profile is shown below in figure 18.

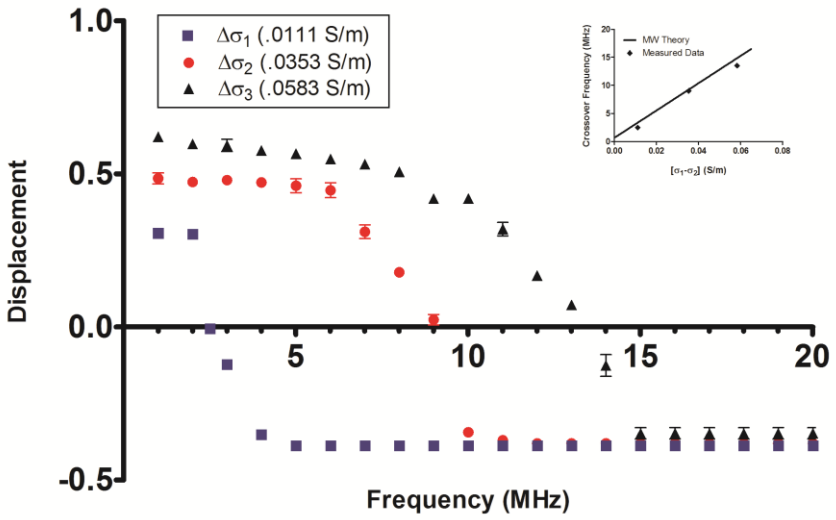


Figure 18: Normalized fluid displacement vs. frequency for change in conductivity. By changing the concentration of PBS we changed the conductivity difference between the two streams. Using a 15V AC field we measured the displacement of fluid from 1MHz to 20MHz. When the displacement is zero, the system is at the *cof*. We determined the location of the interface with a florescence intensity measurement tool in Nikon Elements.

We can also change the permittivity of the AHA while keeping the other electrical properties constant by diluting the AHA with DI water. The resulting decrease in conductivity of the AHA due to the added DI water was too low to detect on the handheld

conductivity meter. The resulting crossover frequency measurements for solutions with permittivity difference $[\varepsilon_2 - \varepsilon_1]$ are shown in figure 19 below.

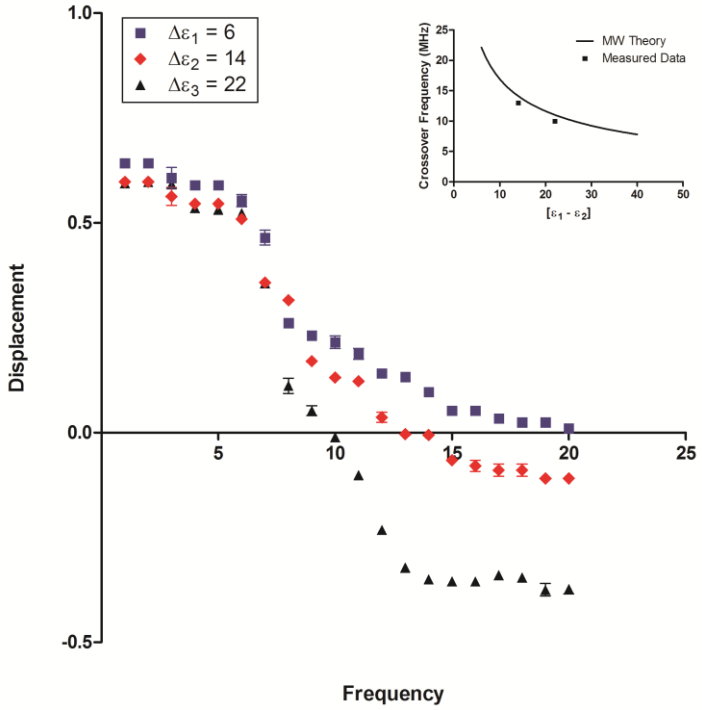


Figure 19: Normalized fluid displacement vs. frequency for fluids for change in permittivity. We diluted AHA from its max permittivity of 110 with DI to change the permittivity difference. The cof is the point was the normalized displacement is zero. The cof increases exponentially as shown in the theoretical graph in the upper right hand corner.

The normalized deflection was calculated using the florescence intensity tool in Nikon Elements. It is clear that because the conductivity difference was not changing, the deflection at low frequency is about the same for all three experiments. As the permittivity decreases the cof rises exponentially as shown in the theoretical graph in the corner of figure 19. The lower the permittivity difference the less force that is applied to the interface. We can see that at high frequency the displacement is lower for decrease in

permittivity. For the final measurement we were not able to find the cof because our function generator stopped at 24 MHz.

As shown in figure 18 and 19, the experimental liquid cof data agree well with the theoretical models. These results strongly suggest that frequency dependent displacement at a polarized aqueous liquid interface is driven by the interaction between the electric field and field induced interfacial charge induced through MW polarization. This interaction produces a net Maxwell stress at the electrical interface, and displaces fluid into the adjacent stream. The direction of this displacement is dependent on the sign of the induced charge; displacement reverses above the cof where the interface undergoes conductive relaxation and charging becomes dictated by differences in dielectric constant at the interface.

A large field confocal image of the electrical displacement shows how the deflection develops down the axial length of the channel. In figure 20 below the dotted line represents the original position of the interface when the field was off.

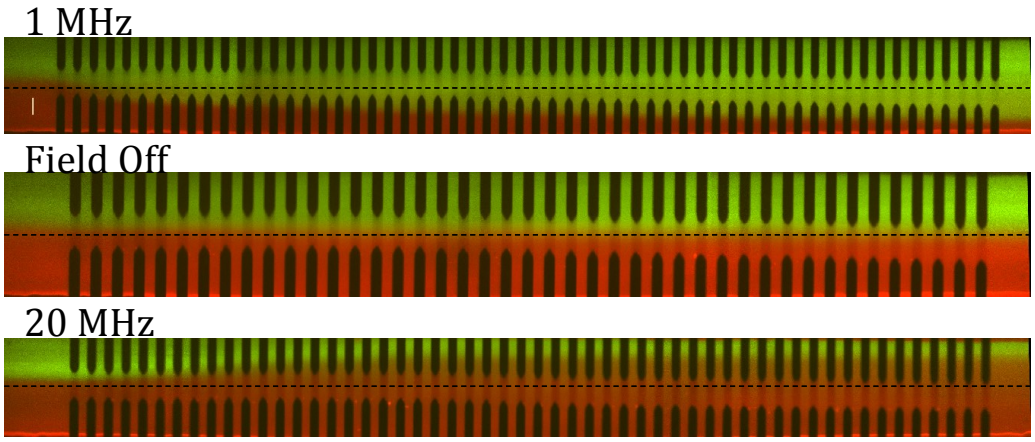


Figure 20: Large field confocal image of deflection at different frequencies. The dotted line is the interface position when the field is off.

From these large confocal images we measure the displacement of the interface down the axial length. The results for 4 different AC voltages are shown below in figure 21 for a fixed frequency of 1MHz.

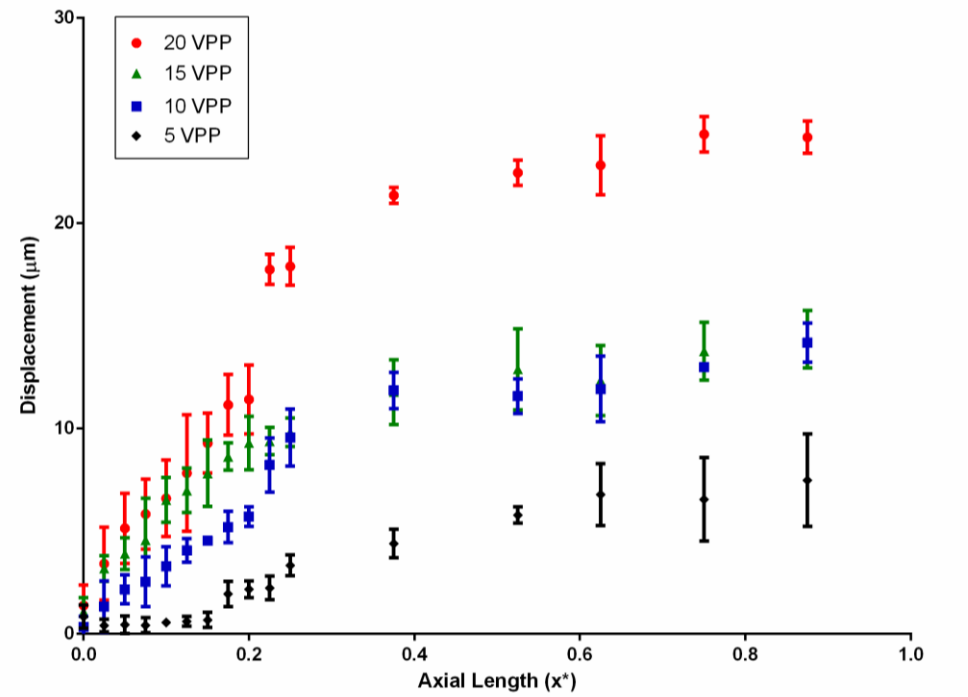


Figure 21: Displacement of interface down the axial length of the channel at 1 MHz fixed frequency. The measurements are taken in triplicate. The interface location is determined with the Nikon fluorescence intensity measurement tool.

The displacement should be increase continuously down the axial length of the channel because there is a continuous force being applied from the electric field. However, there is a very clear leveling off of the displacement after about forty percent of the total length of the channel. This can be explained by looking at the electric potential profile created by the surface electrodes. Comsol Multiphysics creates electric field lines that are coming from the electrode tips shown in figure 22 below.

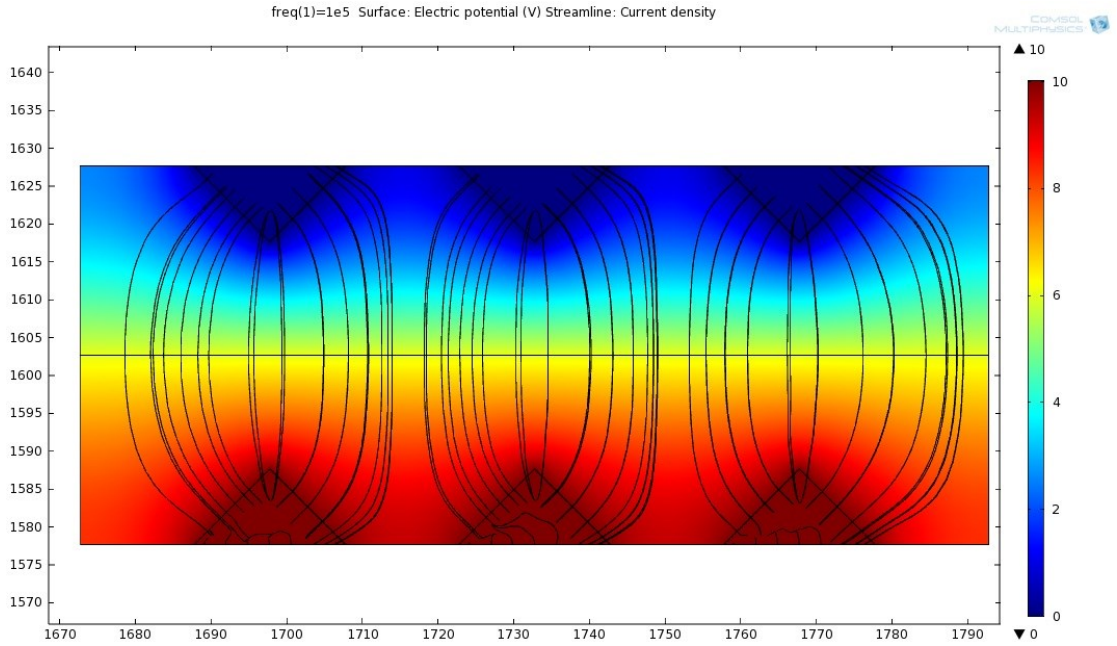


Figure 22: Comsol Multiphysics model of electric potential lines. We designed the electrodes to have points so that the electric field would concentrate at the ends and also to create a more non-uniform electric field.

The electric field coming from the electrodes is focused at the end. When the interface displaces past the electrode tip, there is a great decrease in electric field strength felt by the interface. The decrease in field potential causes the displacement to slow down or stop while going down the channel. Figure 23 below shows only the displacement down the axial length of the channel that takes place between the electrodes.

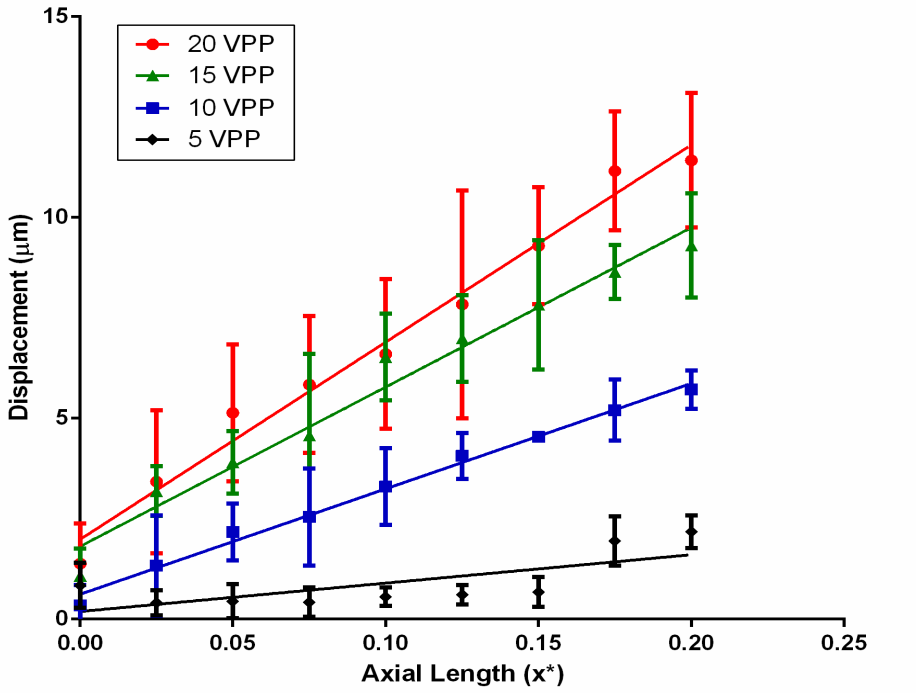


Figure 23: Displacement of interface down the axial length for the 20 $\mu$m region between electrodes.

There is a linear displacement of the interface between the electrodes. To analyze horizontal velocity of the interface due to the electric field between the electrodes we have to correlate axial length to time. By following a single point moving down the channel we can create a moving frame for the interface in the electric field. The first electrode is set to be time zero. Based on the flow rate of fluid coming out of the exit tubing we calculate that it takes about 553 $\mu$s for a moving frame to pass each electrode. From the large image we calculate the velocity of the fluid down the axial length. The velocity profile of the fluid moving between electrodes is shown in figure 24 below.

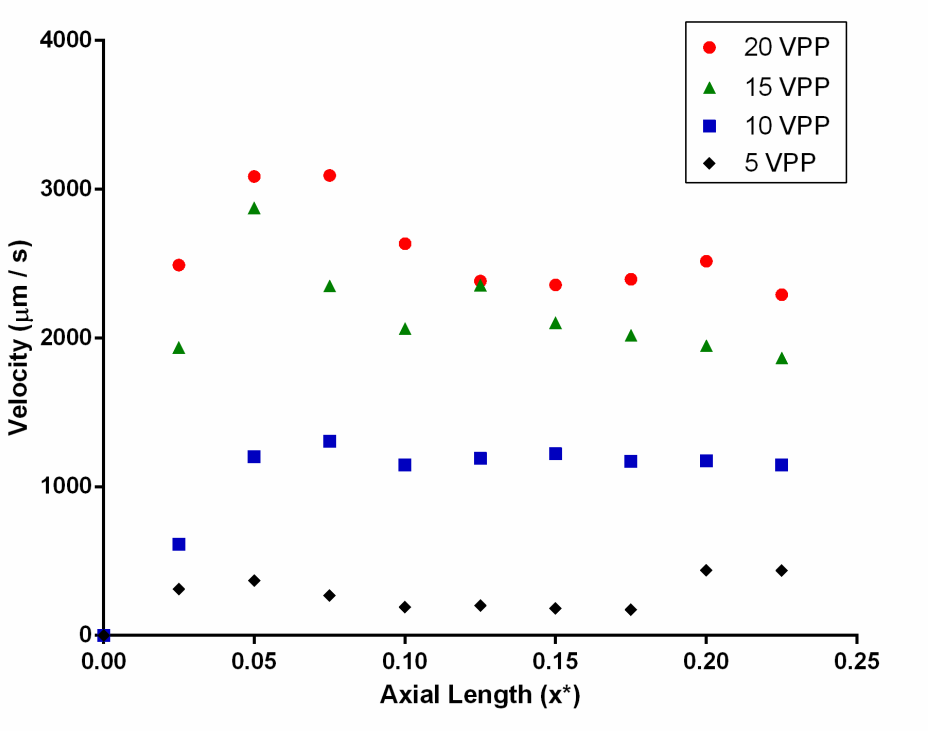


Figure 24: Velocity profile of electrical interface down the axial length of the channel. These velocity measurements are only for points were the deflection stayed between the electrodes. All measurements are at fixed 1 MHz.

There is an initial acceleration at the beginning of the electrodes when the interface first enters the electric field. The velocity of the fluid reaches steady state and is constant after about ten percent of the axial length. No points that displaced past the electrode tips were used because the electric field drops off and the force on the interface decreases. Figure 25 below shows the average velocity for each voltage used, based on the velocity profile above.

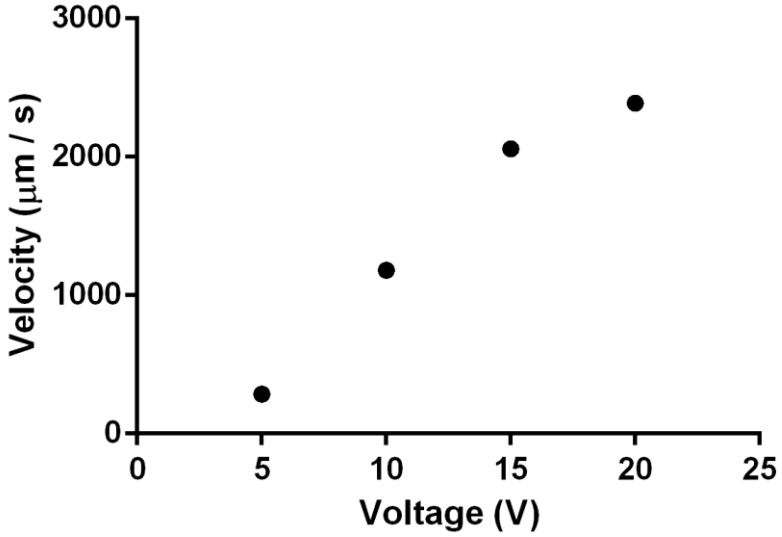


Figure 25: Average steady state horizontal velocity of the liquid/liquid interface for specific voltages.

## COF detection with Impedance

To characterize the interdigitated sensor electrodes that we placed below the fDEP electrodes we recorded the impedance profile over a large range of frequencies. The original frequency range was too large where most of the graph at low frequency was exponential. We narrowed in the frequency sweep to the range 100 Hz to 6 MHz and recorded the impedance every 2000 Hz. The impedance analyzer measures magnitude and phase angle together and exports the results to an excel document. The results of the narrowed sweep are shown in figure 26 below.

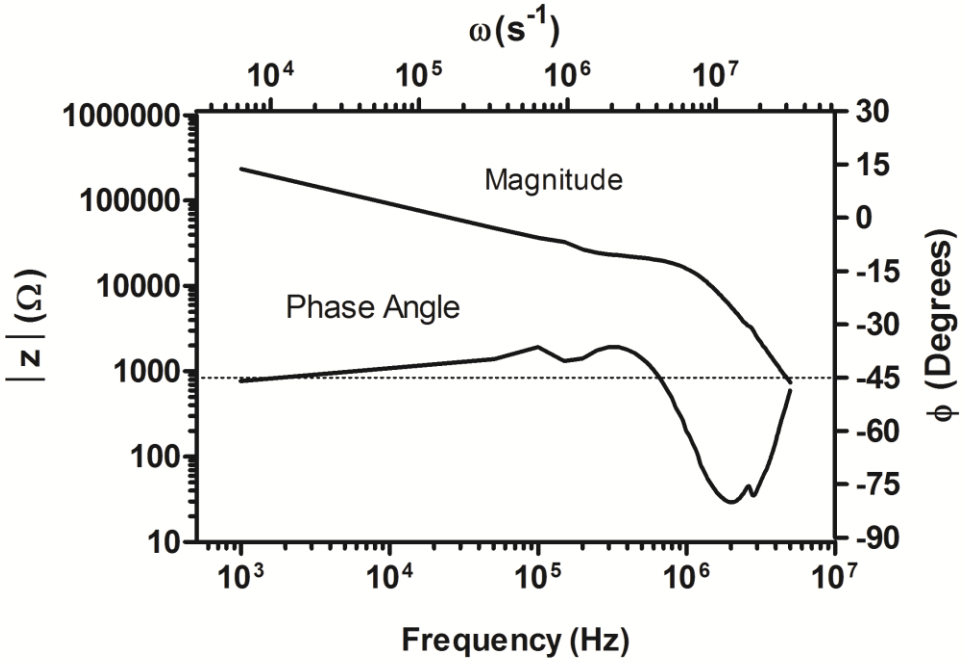


Figure 26: Impedance sweep of liquid/liquid interface. The upstream electric field was turned off and the AHA-PBS interface is set in the middle of the channel.

For these impedance measurements half the channel has AHA and half the channel has PBS. There is a conductivity difference of .035 S/M and the upstream fDEP electrodes are off. For most of the frequency range the phase angel is around -45 degrees meaning that half the impedance is cause by resistance, and the other half is caused by reactance. From this data we can easily calculate the magnitude of the real and imaginary components of the impedance using equation 11 and 12. The magnitude of the resistance and reactance are graphed below in figure 27.

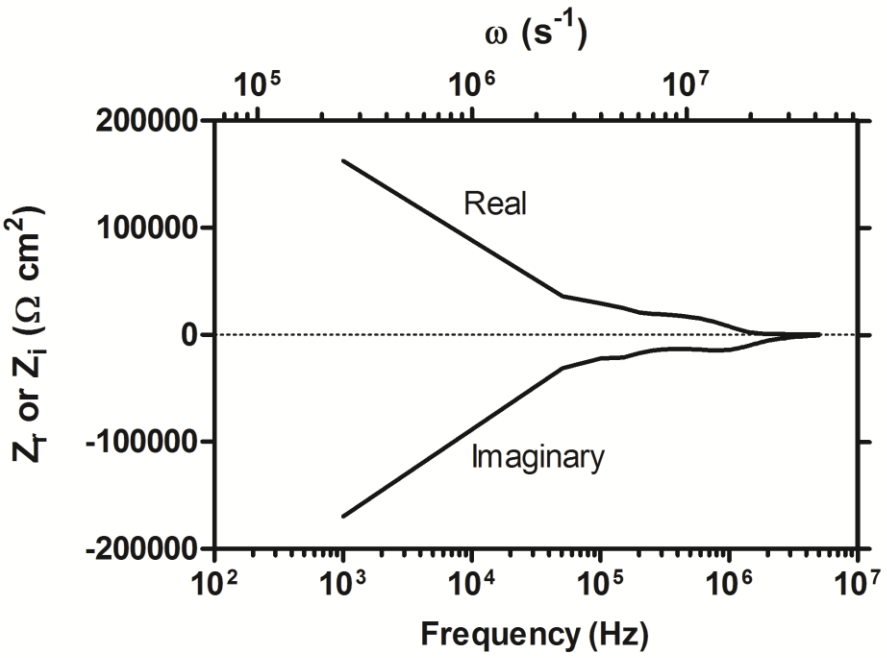


Figure 27: Real and imaginary components of the frequency sweep. This data was taken in the microchannel half AHA and half PBS solution.

The real part of impedance represents the resistance of the system ($Z_r$). The imaginary part represents the reactance of the system ($Z_i$). From this graph we can see that there are equal parts of reactance and resistance for most of the frequency. To further determine the optimum frequency for interface detection we need to repeat the frequency sweep for the other two cases that will exist when the up stream electric field is activated. When we turn on the up stream AC electric field to 1 MHz 15 Vpp the more conductive PBS stream deflects across the bottom of the channel. Downstream from this deflection our impedance sensor is now covered by mostly PBS. The increase in high conductive solution allows charges more charge to move between the sensor electrodes and the impedance decreases, as shown in figure 28 below.

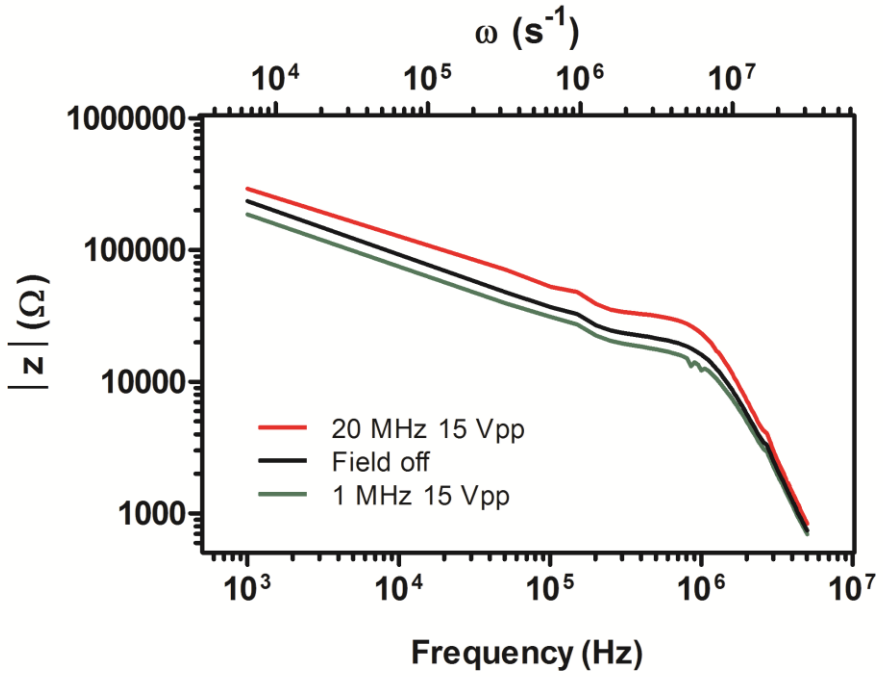


Figure 28: Frequency sweep for interface deflection. When the up stream AC electric field deflects the interface at low frequency, more conductvie PBS solution is on the bottom of the channel than low conductive AHA solution. The increase in conductivity decreases the impedance. At high frequency the low conductive AHA stream defelects on the bottom of the channel and the sensor electrodes are covered by a less conductive solution. The decrease in conductivity increases the impedance.

When the upstream AC electric field is set to 20 MHz and 15Vpp the AHA solution deflects on the bottom of the channel. The sensor electrodes are now covered by mostly low conductive solution. The current traveling between the interdigitated electrodes has more resistance in a low conductive solution and the capacitive effect of the electrode pads decreases. The overall impedance increases when AHA covers the sensor electrodes. It is important to note that the change in impedance is not due to change in flow rate. The flow rate is held constant and only the percentage of PBS and AHA covering the class surface in the channel changes. From the three frequency sweeps we can see that there is a wide range of frequencies that can provide detection of

a moving interface. The frequency with the highest difference in impedance is at 400 kHz.

We use the constant measurement program to record impedance of the sensor electrodes at a fixed signal of 400 kHz and 1 Vpp. The Function generator, attached to the up stream electrodes, is used to sweep the interface in the fDEP range. The function generator starts at 1MHz and goes up to 19MHz at 15Vpp over a 27 second interval so that the frequency changes by 1MHz every 1.5 seconds. The impedance analyzer takes a measurement every 1.5 seconds so by using the above sweep we can match each impedance measurement to a specific frequency that was applied to the interface. The impedance measurements are recorded and graphed below against time in figure 29. On the top axis we correlated the time to frequency.

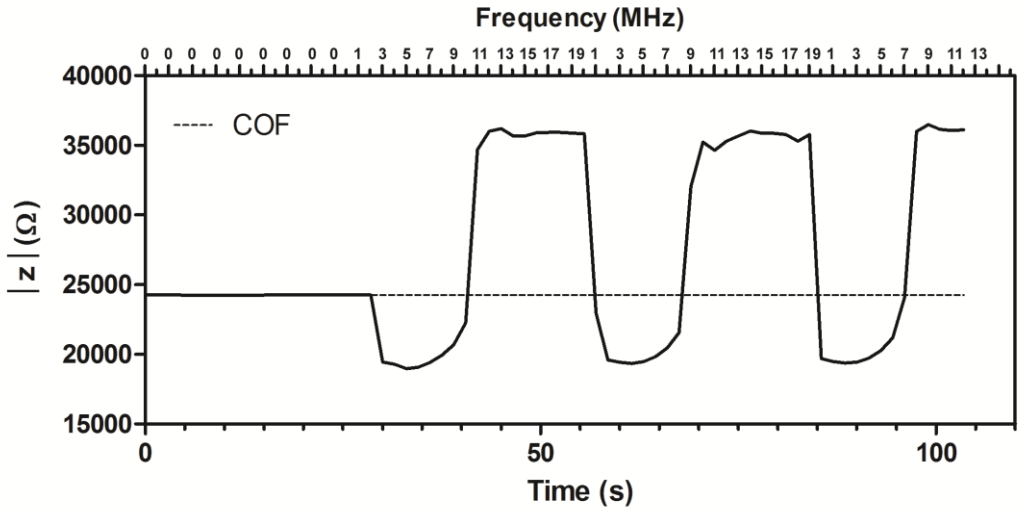


Figure 29: Function generator sweep of the interface recorded by the impedance analyzer at a fixed frequency of 400kHz. The interface above the sensor electrode is shifted to the left (PBS deflection) and then to the right (AHA deflection) due to the upstream low frequency and then high frequency respectively. The dotted line represents the neutral position of the interface with equal amounts of AHA and PBS.

For the first 25 seconds the up stream field is off and the interface is centered in the channel. The dotted line extends the region where the interface is centered. When the function generator is turned on it starts at 1MHz, and the interface shifts left as PBS is deflected. The impedance drops because of the increase in conductivity. The frequency from the function generator is continuously increasing and eventually the cof of the two solutions is reached and the interface is back in the middle of the channel. This is represented on the graph as the impedance measurement crossing the dotted line. On the top axis the frequency applied to the interface when it reached the center is 9MHz. The conductivity difference for these two solutions is .035 ms/cm and the cof should be about 9 based on the theoretical graph in figure 3. It is clear that there is some error in this system because the cof from the graph is not consistent for all three sweeps. The cof on the third sweep is measured as 7MHz indicating that there is some lag in the impedance measurements.

To gain a better understanding of the contribution of each element to the total impedance we can make an equivalent circuit model to describe the physical system. Resistors and capacitors in series or in parallel are applied to each component in the system. Haochen Cui et al. use a very similar electrode design for the detection of tuberculosis (12). Although their electrode design involves a chemical reaction on the surface and only one solution, we can change what the components of the equivalent circuit represent to fit our system. The equivalent circuit model is shown below.

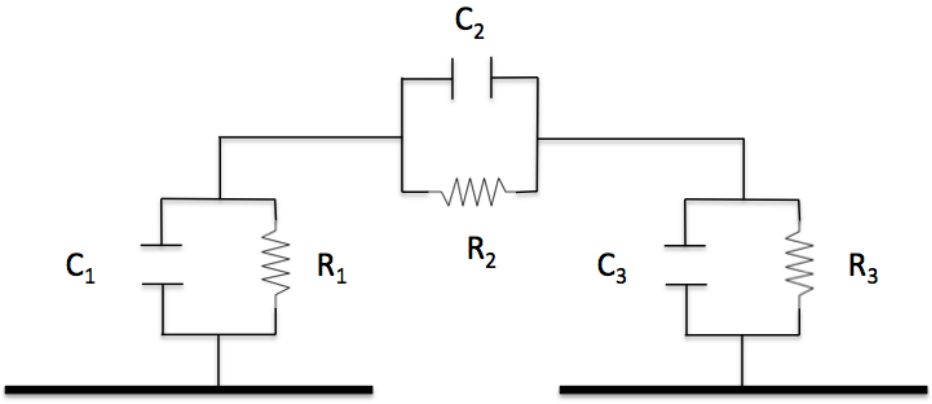


Figure 30: Equivalent circuit model for AHA and PBS flowing in a microchannel. The blocks represent resistors and the parallel lines are capacitors. The system is three capacitors in parallel with three resistors.

There are three capacitors in parallel with three resistors. The parallel capacitors ($C_1$, $C_2$) and resistors ($R_1$, $R_2$) above the electrode represent the solid/liquid interface capacitance and the charge transfer resistance to the electrode respectively. The capacitance of the liquid/liquid interface is represented as $C_2$ and the resistance of the two liquids is represented as $R_2$. From this diagram we can calculate the total impedance of the system as

$$Z = \frac{1}{\frac{1}{R_1}+j\omega C_1} + \frac{1}{\frac{1}{R_2}+j\omega C_2} + \frac{1}{\frac{1}{R_3}+j\omega C_3} \tag{15}$$

were $C_2$ is the interface capacitance. We can model the interface as a capacitor with two different dielectrics. The equation for interface capacitance Cint is

$$C_{int} = \frac{\varepsilon_o A}{\frac{d_1}{\varepsilon_1}+\frac{d_2}{\varepsilon_2}} \tag{16}$$

where $d_1$ and $d_2$ are the distances of each solution between the electrodes, A is the cross-sectional area, and $\varepsilon_o$ is the vacuum permittivity.

We calculate impedance for this equivalent circuit model over the same range that we recorded impedance when the electric field was off in our system. We can then use EIS Spectrum Analysis software to see how well the theoretical impedance from the equivalent circuit model fits our real data. This software varies the value of the capacitance and resistance to get a better fit to the recorded data. The best fit for the equivalent circuit model and our real data is shown below in figure 31.

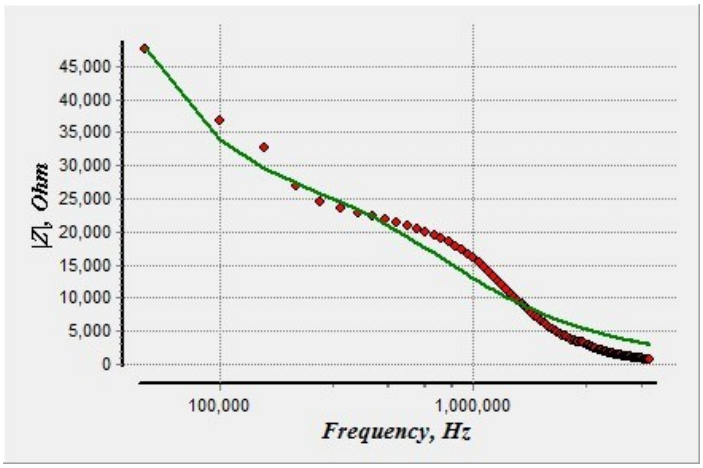


Figure 31: Impedance values calculated from equivalent circuit model fit to impedance measurements taken with no deflection. Our experimental data shown in red was taken when the upstream deflection field was off. The calculated impedance values for the equivalent circuit model are shown in green.

The impedance calculated from the equivalent circuit model is shown in green and the data we recorded from the impedance analyzer is shown in red. The calculated capacitance and resistance for the system when we achieved the best-fit curve are shown below in figure 32.

| Component | Value | Error |
|---|---|---|
| $C_1$ | 12.3 pF | 9.958 |
| $C_2$ | 9.04 pF | 18.293 |
| $C_3$ | 0 | |
| $R_1$ | 23445 Ω | 9.14 |
| $R_2$ | 77054 Ω | 75.59 |
| $R_3$ | 373.42 Ω | 167.06 |

Figure 32: Calculated capacitance and resistance when the equivalent circuit model fits the recorded impedance. These values were calculated by EIS Spectrum Analysis software.

There are problems with the fit of our equivalent circuit model to the recorded impedance as seen by the error values above. This error is mostly due to the connection of the impedance analyzer to the chip electrodes. The wires from the impedance analyzer were connected to the electrodes with solder and standard wire, but we did not include the impedance of these wires in our model.

## Active mixing

As mentioned before, the mixing occurs when the high conductive streams inject inward simultaneously and meet at the center, underneath the low conductive stream. When the two streams hit in the center, they push upward. The symmetry of the side stream injection is disrupted by the inherent offset of the two streams. One of the two streams is slightly larger due to imperfect symmetry, and this stream will dominate by flowing over the other stream and creating micro vortices as shown in figure 33 below.

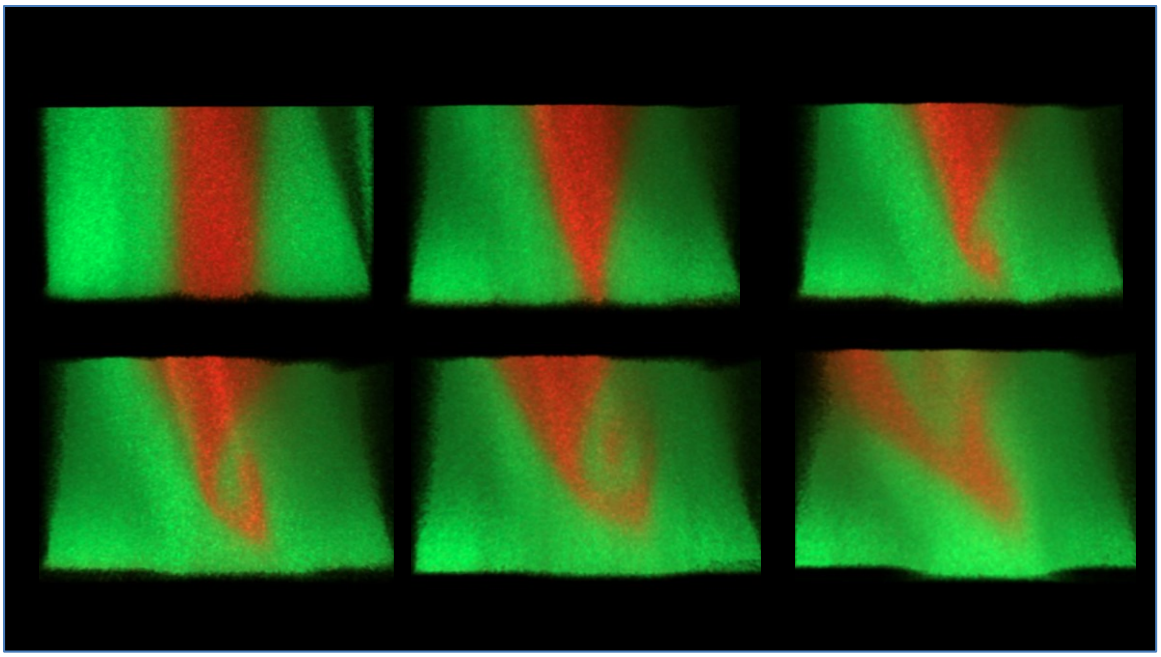

Figure 33: Cross section view of micro vortices cause by two high conductive streams injecting into a center low conductive stream. There will always be one high conductive stream that is slightly larger and that stream will dominate the injection.

These cross-sectional images are taken at the very beginning of the electrode in the first 50 $\mu$m of the electrode design were most of the mixing occurs. Eventually the interface is so disrupted that there is no longer a conductivity difference and mixing stops because there is no more force on the liquid from the applied electric field.

A large view confocal image of the mixing shows us how the mixing develops over time. The first image is the bottom of the channel, the second is 20 $\mu$m above the electrodes, the third is 40 $\mu$m above the electrodes, and the last image is the top of the channel.

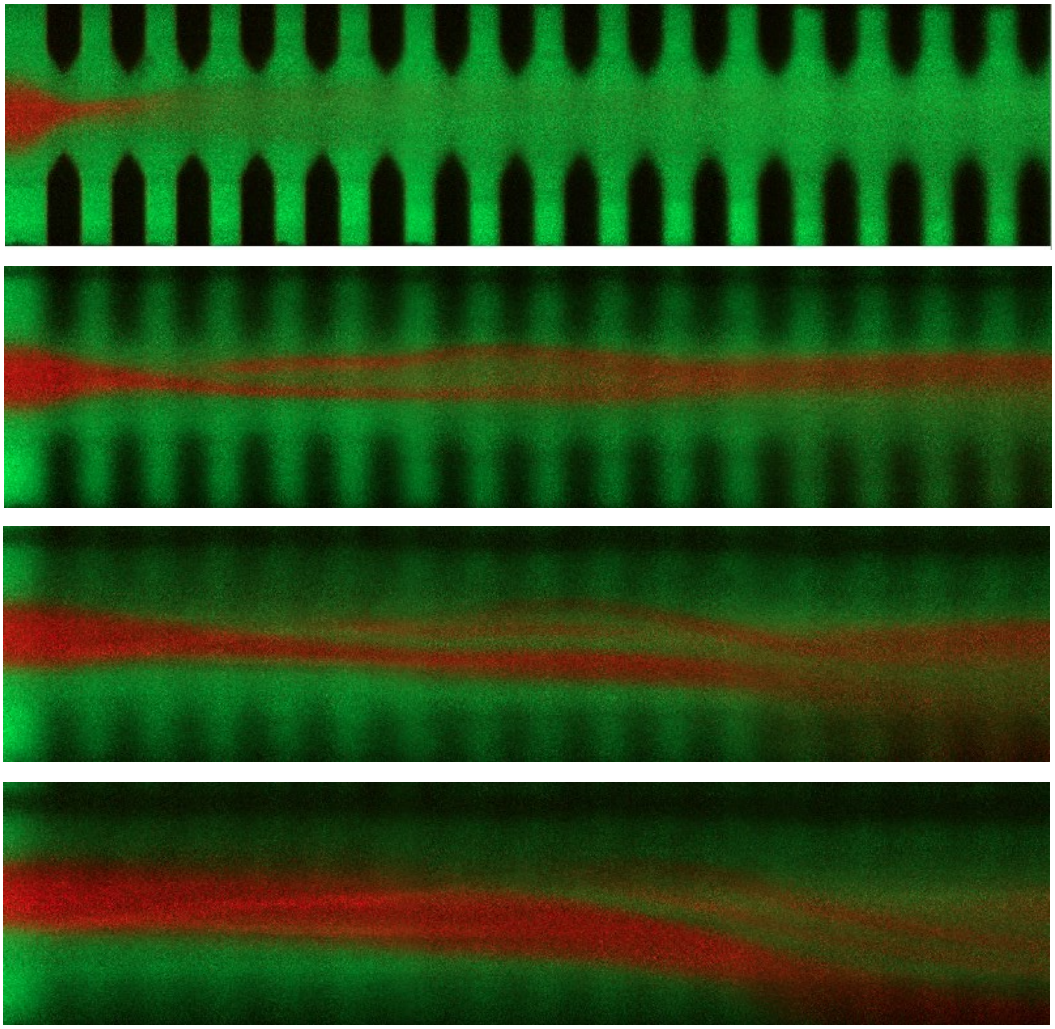

Figure 34: Confocal large image of mixing flow development down the channel. Each picture is a single plane across the microchannel.

At the end of the electrodes we see the overall effect of the mixing. Below are two max intensity projections of z-stack images taken below the electrodes. The NIS florescence intensity tool is used to show to characterize the change in AHA concentration.

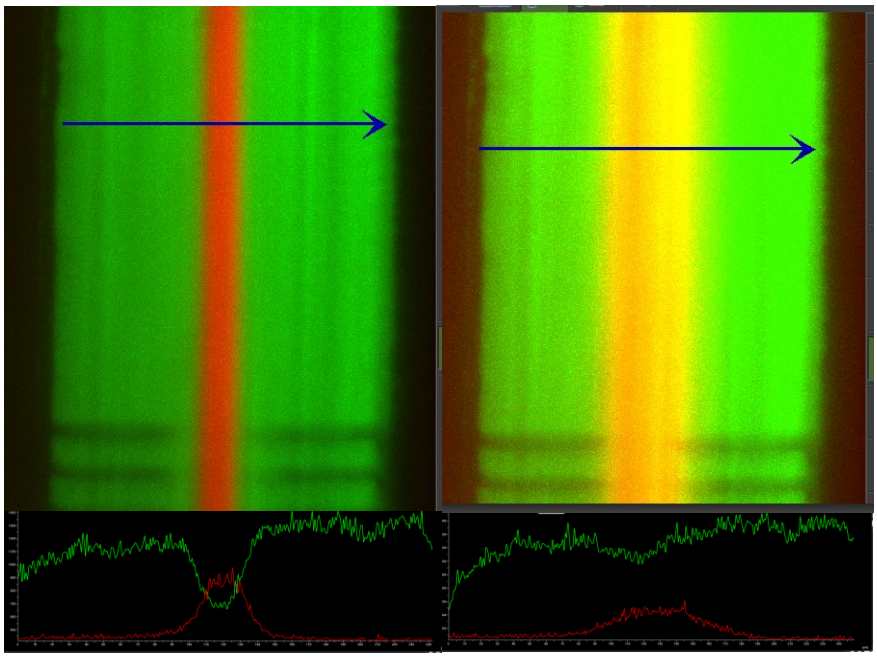

Figure 35: Max intensity projection of confocal z-stack. The left picture shows the fluorescence intensity when the field is off. The right image shows the fluorescence intensity profile when the field is on at 20V ac.

The cross section of these two z-stacks is shown below. It is clear that the center section of the channel that has the AHA becomes diluted with PBS.

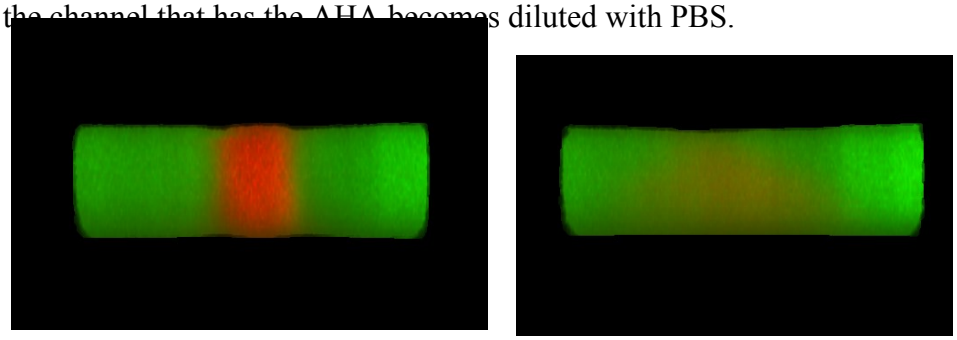

Figure 36: Cross-sectional image of mixing at the end of the electrodes. The left image is field off, the right image is field on.

To determine the extent of mixing and the dependency that the mixing has on voltage we analyze confocal cross-sectional images 50 $\mu$m down the channel. With the faction generator amplifier we are able to analyze the effects of mixing up to 50 V AC. The figure below shows the confocal channel cross-section for field off 10-50 V AC in increments of 10 V.

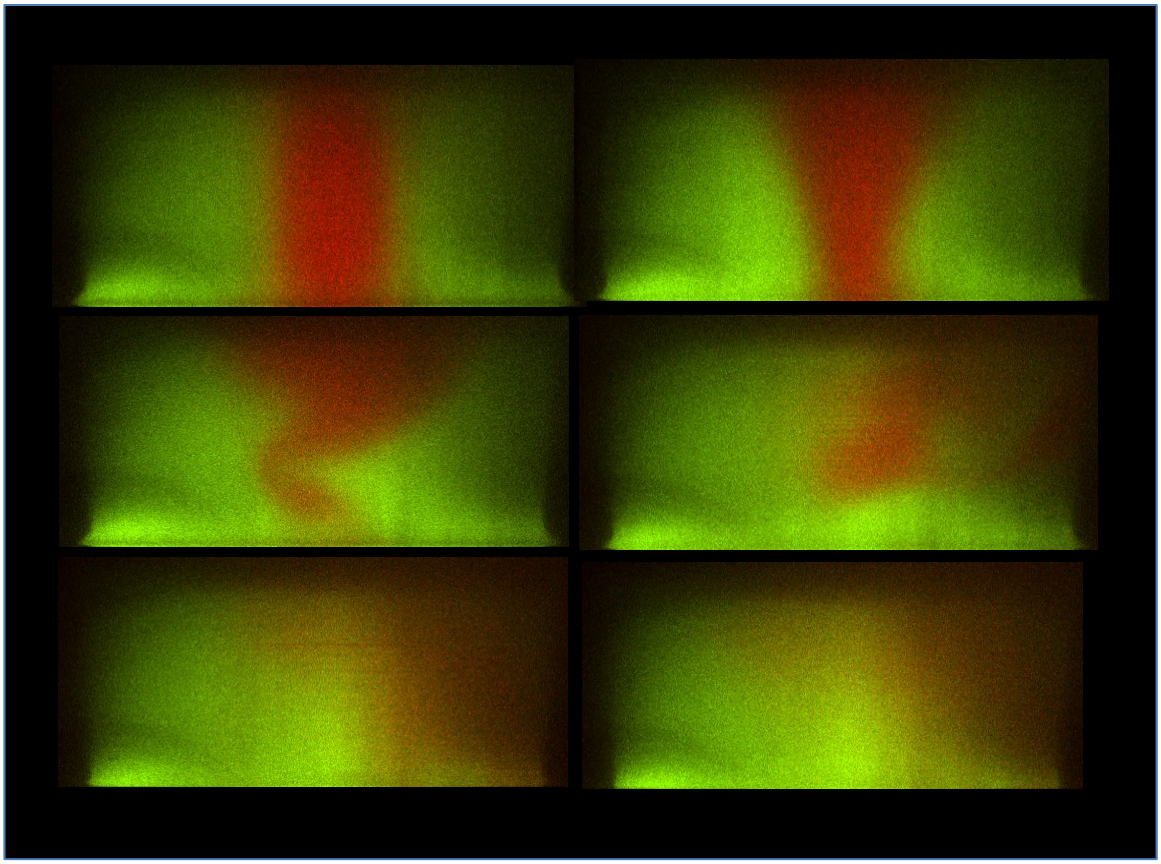

Figure 37: Cross-sectional images to characterize voltage dependency of mixing. The electric field is applied at the bottom. The first figure is when the field off and each additional cross section is an additional 10V ac.

To analyze the mixing based on florescence intensity, each cross section of the channel is broken into three regions, for each of the streams, and is analyzed using Nikon Elements software for fluorescence intensity. The results were normalized so that 1 is the maximum intensity of the green and red, and 0 is the background noise calculated for

each color. The resulting change in fluorescence intensity for the center region, where the red stream is when the field is off, is shown below.

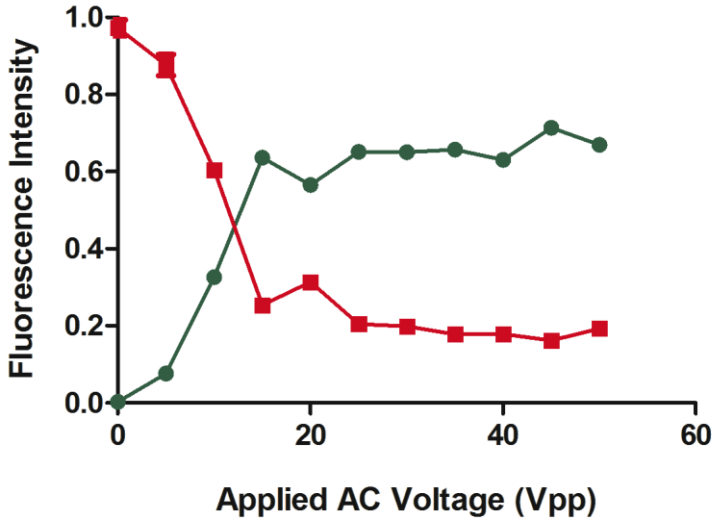


Figure 38: Change in fluorescence intensity for the middle of the channel at different applied AC voltages.

In the middle of the channel there is a clear change in the amount of red and green fluorescence. We create strong mixing at about 15 V and the mixing does not increase after that because the interface is gone and no more force is present from the electric field.

## Chemotaxis Device

Based on this controllable injection of aqueous liquid across liquid/liquid interfaces using an AC field, we demonstrate the ability produce tunable spatial chemical gradients with user-defined geometry, steepness and concentration in a microfluidic device for studying directed cell migration. This is possible because our device utilizes upstream fDEP to control downstream concentration. By changing the applied voltage

and the inlet this voltage is applied to, we can control concentration and direction of a chemical gradient. Below is the injection of cAMP to a downstream gradient device.

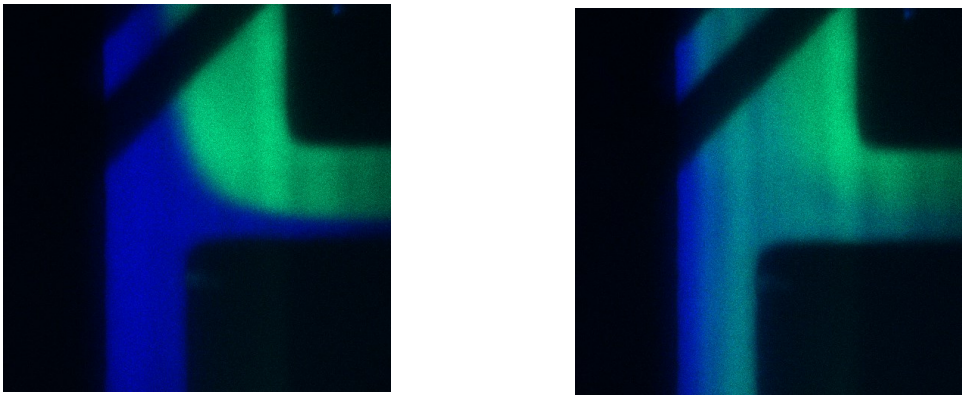

Figure 39: Injection of cAMP (green) to a downstream chemotaxis chamber.

The blue stream is low conductive cell buffer that is normally the only fluid flowing down the channel when the electric field is off. The green stream is high conductive cell buffer with cAMP and normally passes out of the chip, in the channel going to the left, when the electric field is off. When the field is on the high conductive cell buffer injects into the low conductive stream and enters the channel going down. This creates a gradient of cAMP in the down stream component of the device.

We determine the amount of cAMP that is being passed downstream by analyzing the cross-sectional fluorescence intensity. Below is the injection of cAMP based on the frequency applied to the electrodes.

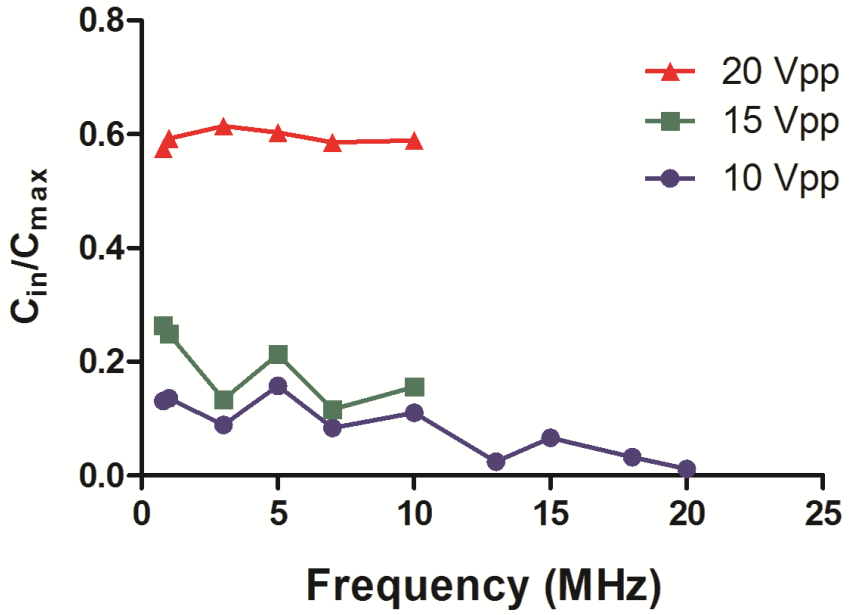


Figure 40: Injection of cAMP to gradient vs. applied frequency to the electrodes. The injection of cAMP was determined from the cross-sectional images take above the gradient portion of the device. The concentration of cAMP was normalized to the maximum amount of cAMP that could be injected, which is the concentration of cAMP in the high conductive buffer stream.

The injection of cAMP was normalized to the concentration of cAMP present in the high conductive cell buffer solution (Cmax). The amount of cAMP that was injected downstream (Cin) was determined from the green fluorescence intensity being sent downstream in the cross-sectional images. The injection is not as dependent on frequency at higher voltages.

We also calculated the amount of cAMP being injected downstream for three different applied AC voltages at a fixed frequency of 5 MHz. The results of these measurements are shown below.

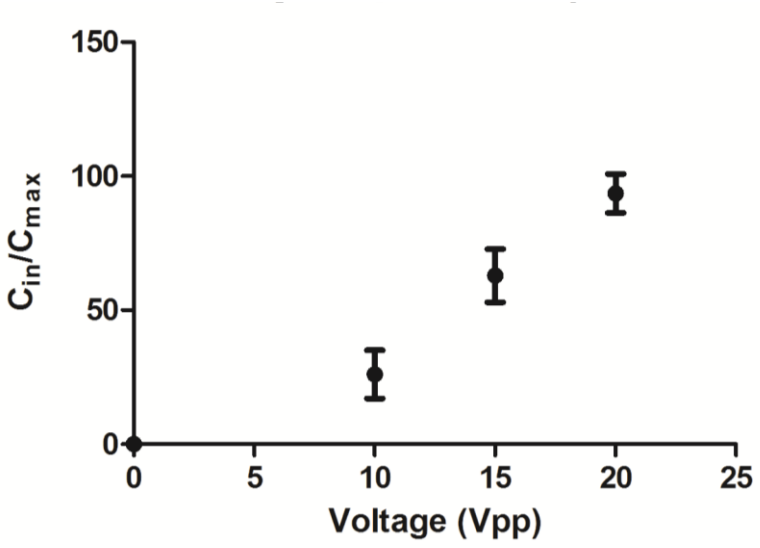


Figure 41: Dependence of downstream cAMP concentration on applied voltage at fixed frequency of 5MHz. $C_{in}$ is the concentration of cAMP injected downstream and $C_{max}$ is the concentration of cAMP in the high conductive cell buffer stream.

Again, the concentration of cAMP is related to the fluorescence intensity of the green high conductive cell buffer solution. The amount of injected cAMP ($C_{in}$) is normalized to the maximum concentration that could be injected if the entire high conductive cell buffer was sent downstream. There is a very linear relationship between the applied voltage and the amount of injected solution.

# Conclusion

We demonstrate that a microfluidic-generated electrical interface formed between two liquids of disparaging electrical properties undergoes interfacial polarization and frequency dependent liquid displacement when exposed to a perpendicular AC electric field. The crossover frequency where no displacement is observed is well described by the Maxwell-Wagner polarization model, and has been experimentally shown to increase when the conductivity difference between the two liquid streams is increased. A liquid stream with greater electrical conductivity and lower permittivity than the adjacent stream is observed to displace across the interface into the lower conductivity phase at frequencies below the interfacial crossover frequency. At high frequencies, above this value, the direction of fluid displacement reverses; the high permittivity fluid displaces into the adjacent low permittivity stream. The interfacial crossover frequency, dependent on the differences between fluid electrical properties between each stream, is observed at an intermediate frequency where no liquid motion is observed and the interface appears identical to when no electric field is applied. These results are similar in nature to the classic crossover frequency behavior observed in dielectrophoresis (DEP), where polarized particles migrate towards high (positive DEP) or low electric field regions (negative DEP) depending upon the AC frequency applied (1). Understanding and exploiting the physics of AC polarization at liquid electrical interfaces could give rise to new ways of precisely manipulating, electrically characterizing and performing fluid biosensing at the nano and picoliter scale, much the same way that DEP is currently utilized to concentrate particles and cells (19), and crossover frequency measurements are exploited in biosensing applications (6). Additionally, this work offers a new method to

more precisely study interfacial polarization, as unlike the solid/liquid interface, the electrical properties in each liquid stream can be readily and independently controlled.

We demonstrate a new type of dynamic microfluidic cell migration and chemotaxis assay that uses fDEP to control solute concentration on-chip. Based on this controllable injection of aqueous liquid across liquid/liquid interfaces using an AC field, we demonstrate the ability produce tunable spatial chemical gradients with user-defined geometry, steepness and concentration in a microfluidic device for studying directed cell migration. This is possible because our device utilizes upstream fDEP to control downstream concentration. By changing the applied voltage and the inlet this voltage is applied to, we can control concentration and direction of a chemical gradient. The fluid displacement design is easily integrated into the upstream components of a microfluidic gradient generator. When the electric field is active, the less conductive fluid from the two side streams mixes across the interface and is passed downstream into the device. If the electric field is removed, displacement ceases, and the fluid from the side streams will exit the two side channels and no gradient is generated. Hence, the gradient direction is switched by activating different upstream electrodes.

The future goal of this work is to quantify and analyze the biased migration of *Dictyostelium discoidium* in response to microfluidic-generated cyclic adenosine monophosphate (cAMP) gradients. We anticipate that having tunable concentration gradients will allow the more precise detection of defects in *Dictyostelium*. As we can control solute concentration with electric fields, we envision the ability to coordinate, direct and study *Dictyostelium.* When the electric field is off no cAMP will be directed to the downstream cell chamber, and cells will exhibit random migration. When one

electrode is switched on, cAMP will be directed downstream and cells will direct their movement up the cAMP gradient. Gradient steepness can then be controlled using varying electric field strengths.

After we create a novel chemotactic gradient device and characterize this system with *Dictyostelium*, my final goal is to transition into a more physiologically relevant cancer cell line. With the ability to create an arbitrary gradient geometry at will, we envision the ability to study the effects of dynamic cell gradients on cancer chemotaxis. Better study of cell chemotaxis in an environment that more accurately replicates the dynamic gradient changes in the human body is the first step to finding drug treatment to disable the cell's chemotactic mechanisms. Because of the complexity of metastasis, researchers believe that cancer may migrate in response to other gradients. This LOC design can create dynamic pH, temperature, electrical, pressure, and conductive gradients simply by changing the inlet stream composition.

Roussos et al. have shown that the metastasis of cancer involves many dynamic signaling cascades, and current chemotaxis assays do not replicate biological conditions to the degree that is necessary to understand these processes (13). The understanding of dynamic chemotaxis is lacking, and can provide vital insight to new methods for stopping cancer metastasis. Precise spatial-temporal control of chemical gradients is required to probe deeper into the underlying sensing and regulating mechanisms in response to this environmental cues that cause mutated tumor cells to spread.

Chemical gradients also play an important role in a variety of other physiological events, such as axon guidance, wound healing, and tissue morphogenesis. Moreover,

immune cells use chemotaxis to circulate between the lymphatic systems as well as migration from the blood towards sites of infection. My chemical gradient chip would be a game changer in the study of these biological events by providing a reliable and flexible tool for experiments (13).

The vision of this research is to create point of care medical diagnostic devices that can be used by anyone around the world. This goal can only be achieved by creating a self contained LOC device. Having dynamic liquid interface control, to build tunable gradients, would be a game changing development for control of cell movement in the testing device. LOC technology may soon become an important part of efforts to improve global health, particularly through the development of point-of-care testing devices. In countries with few healthcare resources, infectious diseases that would be treatable in a developed nation are often deadly. In some cases, underdeveloped healthcare clinics have the drugs to treat a certain illness but lack the diagnostic tools to identify patients who should receive the drugs. Paul Yager Et al. believe that LOC technology may be the key to powerful new diagnostic instruments (22). The goal of LOC research is to create microfluidic chips that will allow healthcare providers in poorly equipped clinics to perform diagnostic tests such as immunoassays and nucleic acid assays with no laboratory support. Being able to control cell migration with internal electric fields and liquid/liquid interface manipulation, rather then complex fluid pressure systems, adds the final goal of LOC technology.

# References


1. Gagnon ZR. Cellular dielectrophoresis: applications to the characterization, manipulation, separation and patterning of cells. ELECTROPHORESIS. 2011 Sep;32(18):2466–87.

2. Green N, Ramos A, Gonzalez A, Morgan H, Castellanos A. Fluid flow induced by nonuniform ac electric fields in electrolytes on microelectrodes. I. Experimental measurements. Phys Rev E. 2000 Apr;61(4 Pt B):4011–8.

3. Morgan H, Green NG, Ramos A, Garcia-Sanchez P. Control of two-phase flow in a microfluidic system using ac electric fields. Appl Phys Lett. 2007;91(25):254107.

4. Gagnon ZR, Chang H-C. Electrothermal ac electro-osmosis. Appl Phys Lett. 2009;94(2):024101.

5. Gagnon ZR, Chang H-C. Dielectrophoresis of ionized gas microbubbles: Dipole reversal due to diffusive double-layer polarization. Appl Phys Lett. 2008;93(22):224101.

6. Gagnon Z, Senapati S, Chang H-C. Optimized DNA hybridization detection on nanocolloidal particles by dielectrophoresis. ELECTROPHORESIS. WILEY-VCH Verlag; 2010 Jan;31(4):666–71.

7. Regtmeier J, Eichhorn R, Bogunovic L, Ros A, Anselmetti D. Dielectrophoretic Trapping and Polarizability of DNA: The Role of Spatial Conformation. Anal Chem. 2010 Sep;82(17):7141–9.

8. Giraud G, Pethig R, Schulze H, Henihan G, Terry JG, Menachery A, et al. Dielectrophoretic manipulation of ribosomal RNA. Biomicrofluidics. 2011;5(2):024116.

9. Markx GH, Talary MS, Pethig R. Separation of viable and non-viable yeast using dielectrophoresis. J Biotechnol. 1994 Jan 15;32(1):29–37.

10. Thaokar RM, Kumaran V. Electrohydrodynamic instability of the interface between two fluids confined in a channel. Phys Fluids. 2005;17(8):084104.

11. Hardt S, Hahn T. Microfluidics with aqueous two-phase systems. Lab Chip. The Royal Society of Chemistry; 2012;12(3):434–42.

12. Cui H, Li S, Yuan Q, Wadhwa A, Eda S, Chambers M, et al. An AC electrokinetic impedance immunosensor for rapid detection of tuberculosis. Analyst. 2013;138(23):7188.

13. Roussos ET, Condeelis JS, Patsialou A. Chemotaxis in cancer. Nature Publishing

Group; 2011 Aug 1;:1–15.

14. Skoge M, Adler M, Groisman A, Levine H, Loomis WF, Rappel W-J. Gradient sensing in defined chemotactic fields. Integr Biol. 2010;2(11-12):659.

15. Orazem ME, Tribollet B. Electrochemical Impedance Spectroscopy. 2014. 446 p.

16. Marie ES. AgilentImpedance Measurement Handbook. 4 ed. 2014. 140 p.

17. Suh YK, Kang S. A Review on Mixing in Microfluidics. Micromachines. 2010 Dec;1(3):82–111.

18. Whitesides GM, Ostuni E, Takayama S, Jiang X, Ingber DE. Soft lithography in biology and biochemistry. Annu Rev Biomed Eng. 2001;3(1):335–73.

19. Gagnon Z, Mazur J, Chang H-C. Integrated AC electrokinetic cell separation in a closed-loop device. Lab Chip. 2010 Mar 21;10(6):718–26.

20. Arnold WM, Zimmermann U. Dielectric properties of zwitterion solutions. Biochem Soc Trans. 1993 Nov;21(4):475S.

21. Toetsch S, Olwell P, Prina-Mello A, Volkov Y. The evolution of chemotaxis assays from static models to physiologically relevant platforms. Integr Biol. 2009.

22. Yager P, Edwards T, Fu E, Helton K, Nelson K, Tam MR, et al. Microfluidic diagnostic technologies for global public health. Nature. 2006 Jul 27;442(7101):412–8.

# Resume

EDUCATION

**Johns Hopkins University** **Baltimore, MD**
Masters of Science in Chemical & Biomolecular Engineering Expected Aug 2014

**Johns Hopkins University** **Baltimore, MD**
Bachelor of Science in Chemical & Biomolecular Engineering May 2013
Awards: ChemBE Research Award 2013, ChemBE Excellence Award 2013, Dean's List

EXPERIENCE

**JHU Dr. Gagnon Research Lab** **Baltimore, MD**
*Graduate Researcher* Dec. 2011 - Present

- Coordinated the development of new research lab from concept beginning
- Independently mastered microfluidic techniques in class 1000 clean room
- Structure and Supervise training of new doctoral students and undergraduates
- Progress and analyze research ideas related to point of care microfluidic devices

**CureDM** **Philadelphia, PA**
*Research Assistant* May 2010 – Sep. 2010

- Reviewed and presented on human pancreatic beta-cell expansion from islet cells for treatment of diabetes mellitus type 1
- Pinpointed ideal conditions for in vitro islet cell activation with protein treatment
- Demonstrated activation efficiency of islet cells based on insulin production analysis

**Baltimore City Engineering Outreach Program** **Baltimore, MD**
*Volunteer, Coordinator* May 2013 – Aug. 2013

- Lead summer program to inspire city high school students to pursue engineering studies
- Developed hands on experiments to demonstrate concepts in physics and microfluidics

PUBLICATIONS

"Maxwell-Wagner Polarization and Frequency Dependent Injection at Aqueous Electrical Interfaces" by **Mitchell Desmond**, Nicholas Mavrogiannis, and Zachary Gagnon *Physical Review Letters*. 109, 187602 – Published 23 October 2012.

"A Dynamic Microfluidic Gradient Generator Controlled by Fluidic Dielectrophoresis" by **Mitchell Desmond** and Zachary Gagnon. Advances in Microfluidics and Nanofluidics 2013 - Poster

SKILLS

**Computer**: Microsoft Word, Excel, Power Point, Matlab, AutoCAD, Photoshop, Illustrator, Lab View, Printed Circuit Board, Nikon confocal and TIRF microscope with NIS Elements software

**Lab skills**: Positive and negative photolithography, Electron beam evaporation, Gold etching, Agarose gel electrophoresis, Column chromatography, Protein labeling, Bright field microscopy, Confocal microscopy, Fluorescence microscopy, TIRF microscopy, Centrifugation, pH meter

**Foreign Language**: Spanish (conversational)